Final Research Project in MSc Chemical Engineering

Kinetics of High Pressure Methanol Synthesis

Part of Supermethanol, GtM Project

Author: K.M. Kuipers, S1577417

First supervisor: Prof. dr. ir. H.J. Heeres

Second supervisor: Prof. dr. A.A. Broekhuis

Daily supervisor: Dr. ir. J.G. van Bennekom

university of groningen

faculty of mathematics and natural sciences

university of groningen / faculty of mathematics and natural sciences

Acknowledgement

The major part of the second year of the Chemical Engineering master program is the final research project that will be concluded with a thesis. In this final project, most of the subjects taught in the master program should be combined and used to individually perform this research. The research project runs for a period of nine months and is concluded with a final presentation. The main objective of this thesis was to find the kinetics of methanol synthesis at high pressures, readers that are interested in the abstract of this report are referred to the next page.

I would like to thank dr.ir. J. van Bennekom and E. Wilbers for their help, support, time and their endless patience. Without their advice and participation this thesis would not have been completed. I would also like to thank Prof.dr.ir. H.J. Heeres and dr.ir. J. van Bennekom for providing me with feedback and support during my final research project.

Groningen, March 2014

Karin Kuipers

Summary

In the exploration of renewable energy, biodiesel is coming forward as one of the leading solutions. Biodiesel is produced from a plant oil or fat and methanol, giving crude glycerol as a byproduct. One of the big advantages of biodiesel production is that a local feedstock can provide the required plant oil whereas methanol is a common platform chemical. Production takes place all over the world and its product is available at most European gas stations. Unfortunately, the rapid introduction of biodiesel to the market showed to have an influence on the selling price of its byproduct which decreased considerably between 2006 and 2010. Deterioration of glycerol prices could make biodiesel a lot less economically attractive for its producers. The Supermethanol project was initiated to develop a cost efficient process to reform crude glycerol to methanol in a two-step process by first reforming the glycerol to synthesis gas, followed by the conversion of synthesis gas to methanol.

Methanol is produced on industrial scale at pressures between 5.0 and 10.0 MPa and formed via equilibrium reactions that requires the process to have a recycle stream back to the reactor. The synthesis gas obtained from the Supermethanol reforming process has an approximate pressure of 20.0 MPa, at this pressure the reaction equilibrium tends to full conversion. In addition, the formed methanol condenses in the reactor ensuring full conversion of the reactants. Without the necessity of a recycle stream, the methanol conversion process becomes less complicated and of smaller size which opens a window for implementation into an existing biodiesel plant.

In this study a kinetic model was developed for the synthesis of methanol at pressures of 17.5 – 22.5 MPa based on experimental data obtained from experiments using a commercially available $Cu/ZnO/Al_2O_3$ catalyst. The formation of methanol and water was studied using varying feed compositions of CO, CO_2 and H_2 in a continuous spinning basket reactor by making use of an online gas chromatograph. Three kinetic models, based on a Langmuir-Hinshelwood/Hougen-Watson model and power law model were fitted to the experimental data. Finally, the best fitting model was found to give a relative average error of $\Delta R'_{CH_3OH} =$ 18.4 % for a temperature range of 483 to 498 K.

Many kinetic models for the synthesis of methanol have been published over the last decades. Most of these are developed for low pressure methanol synthesis and are not applicable in the Supermethanol region. The kinetic model developed in this study can be considered the first of its kind.

Table of Contents

1 Introduction

1.1 Supermethanol

Over the last decades, views on energy have changed. Depleting oil reserves and increasing oil prices have reached household discussions and a pending oil crisis pushed governments and academics in the search to alternatives. Research on renewable energy sources is numerous, very much a part of the daily news and still booming. New technologies are developing and some have already taken their place in our daily life in the form of hybrid cars, public transport fueled by biogas or hydrogen and a choice to make between regular- and biodiesel at the gas station.

These developments are very much cheered on by politicians and the European Commission has set targets for the implementation and use of renewable energy in the EU. In the directive set in 2009 the use of biofuels and other types of renewable energy is promoted to be used in the transport sector. Guidelines target a minimum of 10% transportation fuels to be derived from renewable resources by 2020 of which the largest share will be of biodiesel [1] of which production has already increased significantly in capacity in Europe since 2000. Biodiesel is produced from vegetable oil and methanol. In amounts, a ton of product requires roughly 100 kg methanol and produces a similar amount of glycerin as valuable co-product. The increasing biodiesel production also increases the amount of crude glycerin available to the market [2]. As a rule, an increasing new market affects another. Figure 1-1 shows the change in market price of crude glycerin in Europe, the graph shows that the increase in biodiesel production has an immediate effect on the market price of crude glycerin. Methanol prices on the other hand are increasing with an overall of 7 to 8% per annum [3]. Simply said, producing large amounts of biodiesel could consequently lead to economic deterioration of the production. Creative and innovative use of the glycerol byproduct is therefore worthwhile to investigate.

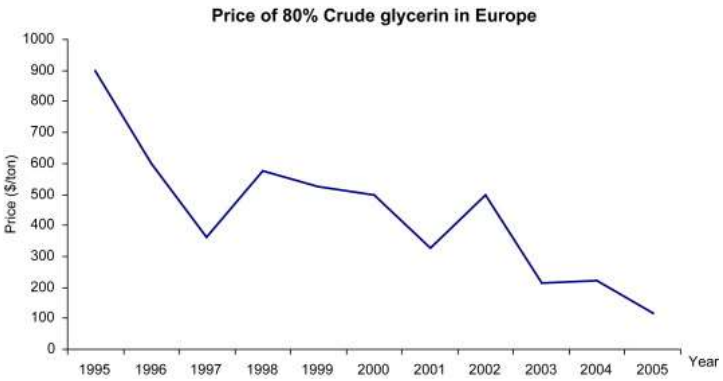

Figure 1-1 Change of market price of 80% crude glycerin in Europe [2]

The Supermethanol project was initiated to develop a cost efficient process to produce methanol from the crude glycerol and integrate this into an existing biodiesel producing facility. Using the byproduct of the process as new feedstock will not only supply the biodiesel production of green, sustainable methanol, implementation will make biodiesel production less dependent on methanol and glycerol market prices. The Supermethanol project is shown as a flow chart in Figure 1-2. Biodiesel is produced by trans-esterification of vegetable oils with methanol in the presence of a catalyst. Crude glycerol byproduct is subsequently reformed to methanol in the Glycerol to Methanol (GtM) process. This process exists of two sub-processes starting with reforming glycerol in supercritical water (RSCW) to syngas, followed by methanol synthesis from the high pressure gas.

Water becomes super critical when it is pressurized above 22.05 MPa and a temperature higher than 647 K. At temperatures over 873 K (600 °C) water becomes a strong oxidant and treating organic material with it results in disintegration of its structure. Transfer of the water molecules' oxygen to the carbon atoms of the organic material results in carbon dioxide, CO_2, and smaller amounts of carbon monoxide, CO. The remaining hydrogen atoms from water and the organic material form H_2. The RSCW process of the Supermethanol project takes place in a reactor operating at temperatures between 873 and 933 K and a pressure around 30 MPA. The residence time is around two minutes, depending on the feed type, for total carbon conversion. A typical overall reaction for glucose can be written as:

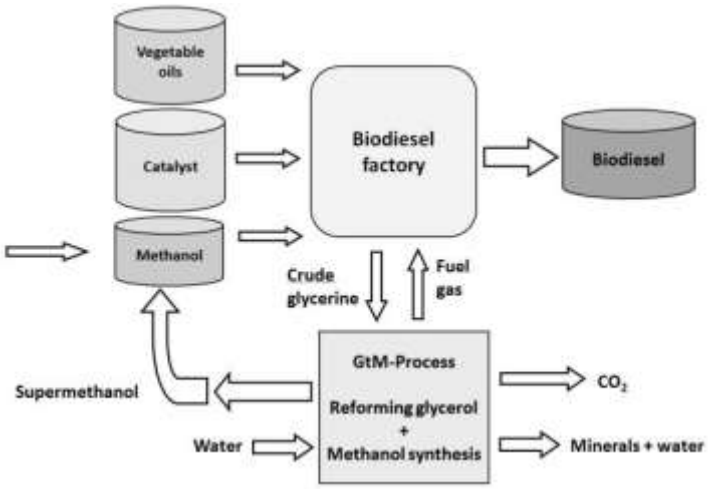

Figure 1-2. Schematic overview of Supermethanol project [10]

$$2\ C_6H_{12}O_6 + 7\ H_2O \rightarrow 9\ CO_2 + 2\ CH_4 + CO + 15\ H_2.$$

The two phase reactor effluent stream is separated easily in high pressure synthesis gas mixture consisting of H_2, CO, CO_2, CH_4 and higher hydrocarbons and a water phase in which part of the CO_2 is dissolved [4] [5]. The second main focus is formation of methanol from the acquired syngas. The high pressure gas is let through a reactor containing a commercial $Cu/ZnO/Al_2O_3$ catalyst where the methanol is formed.

1.2 Introduction to Methanol

Pure methanol was first isolated as a chemical in 1661 by Robert Boyle, produced from distillation of boxwood. Industrial large scale synthesis of methanol however dates back to the 1900's when methanol was almost exclusively produced from wood wastes, from which its trivial name, wood alcohol, originates [6]. In 1923, BASF developed the first commercial methanol production process based on a ZnO/Cr_2O_3 catalyst and synthesis gas. This process operated between 10 - 25 MPa and temperatures of 573 -and 673 K and is today referred to as high-pressure methanol synthesis [7]. This technology was replaced in the 1963 by the low-pressure process, developed by Imperial Chemical Industries Ltd. (ICI). Due to a new technology producing syngas from natural gas and naphta, producing almost sulphur free syngas, it became possible to use new and more active Cu-based catalysts. With the more active catalysts, lower pressures of 5 - 10 MPa and temperatures of 500 - 563 K were adopted [7]. Today almost all methanol producing plants use a low-pressure process. The process design varies based on availability of feedstock, process energy efficiency and economic circumstances. The differences are mostly seen in the reactor type used, either a multi-bed synthesis reactor with feed-gas quench cooling, typical for the ICI process, or a multi-tubular synthesis reactor with internal cooling known as the Lurgi

process. The Halder Topsøe process uses several adiabatic reactors and intermediate coolers are placed to remove the heat of reaction [8].

In 2010 the global demand of methanol was 45.6 million metric tons produced in Asia, North and South America, Europe, Africa and the Middle East [9]. Methanol is an important platform chemical and has potential as a clean and renewable fuel. Methanol is used to produce formaldehyde, a solvent and base in the production of urethane foams and adhesives and methyl tertiary butyl ether (MTBE), an oxygen replacer and enhancer of the octane number in gasoline and also used to replace lead and aromatics. A smaller, but still substantial amount is used for the production of acidic acid of which telepthalic acid, vinyl acetate and solvent esters are derivatives [8] [9]. An overview is given in Figure 1-3.

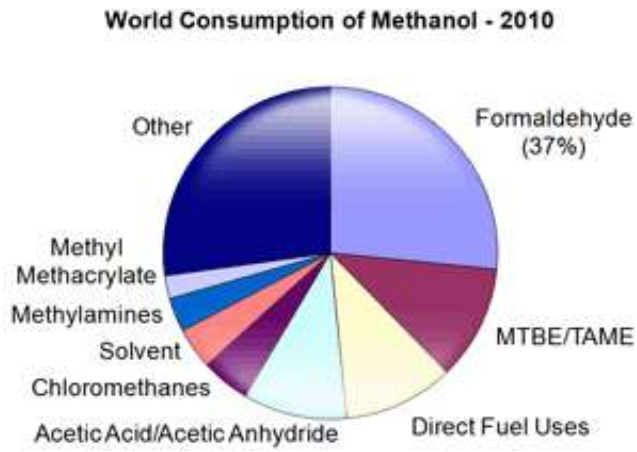

Figure 1-3. Overview of industrial uses of methanol in 2010 [9]

1.3 Methanol Synthesis

Methanol (CH_3OH) is the smallest and simplest alcohol and a light, colorless and flammable liquid at room temperature. Methanol contains less carbon and more hydrogen than any other liquid fuel [7]. Three overall reversible reactions are the basics of methanol synthesis; hydrogenation of carbon monoxide (1), the reverse-water-gas shift reaction (RWGS) (2) and hydrogenation of carbon dioxide (3). Together they form an equilibrium system.

$$CO + 2H_2 \leftrightarrow CH_3OH \qquad \Delta H_{298} = -90.64 \text{ kJ/mol} \qquad (1)$$

$$CO_2 + H_2 \leftrightarrow CO + H_2O \qquad \Delta H_{298} = +41.17 \text{ kJ/mol} \qquad (2)$$

$$CO_2 + 3H_2 \leftrightarrow CH_3OH + H_2O \qquad \Delta H_{298} = -49.47 \text{ kJ/mol} \qquad (3)$$

Methanol is produced industrially from synthesis gas consisting of H_2, CO, CO_2 and small amounts of CH_4, commonly derived from natural gas or coal. With the use of a Cu-based catalyst, CO is preferred over CO_2 as reactant. In practice it is found that for kinetic reasons a minimum of 2.5 to 3.5 % of CO_2 has to be present. The preferable composition of the synthesis gas therefore contains a highest possible CO and lowest possible CO_2 content. The optimal stoichiometric ratio, S_N, of syngas is set on 2.0:

$$S_N = \frac{(H_2 - CO_2)}{(CO + CO_2)} \qquad (4)$$

With S_N equal to 2, all reactants can be converted to methanol. With $S_N > 2$, carbon monoxide and carbon dioxide are limiting components and with $S_N < 2$, hydrogen is limiting [6].

The progress of the equilibrium reactions in methanol synthesis is restricted by thermodynamics For a low-pressure process a syngas conversion of 30-70% is commonly achieved per pass of the reactor, requiring the unconverted syngas to be sent back to the reactor in a recycle stream. An ICI plant has a typical recycle ratio between make-up gas and recycled gas that varies between 1:3 and 1:4 depending on the operating conditions and syngas composition [7].

Figure 1-4 shows the equilibrium conversion of CO + CO_2 in several processes as a function of temperature at different pressures for a gas composition of $H_2/CO/CO_2/CH_4$ = 64/24/4/5 vol% (S_N = 2.25) [10]. The synthesis of methanol is exothermic and involves a decrease in number of moles. Le Chateliers principle therefore predicts that the maximum conversion is obtained at low temperatures and high pressures [11]. From the figure it is clearly seen that high pressure and relatively low temperatures are thermodynamically the most favorable reaction conditions [10]. The reaction conditions of the Supermethanol project are very favorable for the reaction equilibrium. Trends in methanol synthesis aim for lower temperature and lower pressure processes. Compression is a costly process and has an economic impact on production cost. Through RSCW high pressure syngas is obtained, in this way the energy intensive compression step is avoided and the high conversion equilibrium would make a recycle streams not necessary. New, more active Cu-based catalysts allow for lower reaction temperatures.

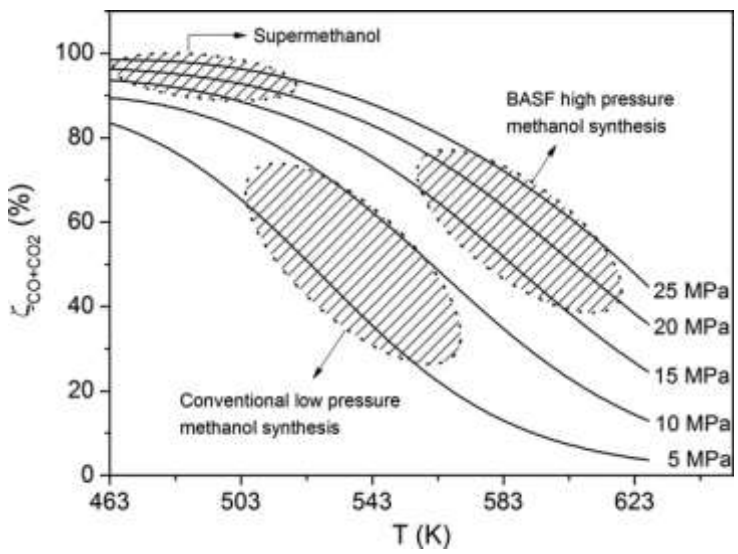

Figure 1-4. Equilibria in methanol synthesis for different pressures (H2/CO/CO2/CH4 = 67/24/4/5 vol% [12]

1.4 Justification and aim of the research described in this thesis

With synthesis of methanol at 20 MPa and 473 K, in situ condensation of methanol has been demonstrated, which drives the equilibrium nearly to completion [12]. This demonstration makes the Supermethanol project a viable and economically feasible process for possible industrial implementation. For reaction conditions like these however, a kinetic equation describing the synthesis is not available. The aim of this research is to obtain kinetic data for methanol synthesis from syngas over a Cu-based catalyst in the high pressure, low temperature region of the Supermethanol project. The goal is to derive a kinetic expression from the collected data as the first in its sort that describes the reaction between 17.5-22.5 MPa and 483-498 K.

Methanol synthesis from syngas is considered a well-established process and the amount of literature on this topic is therefore numerous. An overview of literature and theory used as the base in the research project is given in the following chapters.

2 Literature

2.1 Catalysis

The synthesis of methanol goes via a heterogeneous catalytic reaction. The first commercial catalyst, developed and used by BASF in their high pressure plant in 1923 was ZnO/Cr_2O_3. These types of catalyst are not very active; the process therefore required relative high temperatures to obtain a reasonable reaction rate. The higher temperature, lowering the equilibrium to methanol (see Figure 1-4), was compensated by increasing the reaction pressure. As stated in the Introduction, the high-pressure technology has only been replaced in the 1960's by low-pressure technology when steam reforming of natural gas and naphtha produced a sulphur free syngas feedstock and making it possible to use more active copper based catalysts [7]. The activity of copper in methanol synthesis had been discovered in the 1920's as well as the activity of ZnO. Copper however is easily poisoned by sulphur and very sensitive to sintering, while ZnO is slow and is not very active. A combination of the two catalysts, a co-precipitated CuO/ZnO, was found to poison quickly and sinter due to large crystal conformation with unevenly distributed metals. Irreducible oxides Al_2O_3, Cr_2O_3 and ZrO_2 were than introduced as support; they give small crystals with evenly distributed components. Nowadays, $Cu/ZnO/Al_2O_3$ catalysts are almost exclusively used, they are very stable and remain active for several years under industrial conditions [7, 13]. Methanol catalyst development and preparation routes are largely summarized in [7, 13, 14].

2.1.1 Heterogeneous catalysis

Catalysts can modify the rate and selectivity of a chemical reaction. Methanol synthesis takes place in the gas phase and is catalyzed by solid porous catalyst particles, giving rise to a heterogeneous catalytic system. A porous catalyst particle is schematically shown in Figure 2-1 with the nine steps of a catalytic pathway. Step 1 and 9 are convection, here the reactants displace from the bulk gas mixture towards the catalyst pellet and the other way around. Convection is a macroscopic process transporting components from high to low concentration areas. This step is dependent on the component concentration gradient in the system. Step 2 and 8 are called diffusion and is not a convective process. Diffusion is the random motion of chemical species in a mixture caused by thermally induced agitation of molecules; both convection and diffusion are more intensive at higher temperatures. Diffusional flux of component i can be described by Fick's Law of diffusion:

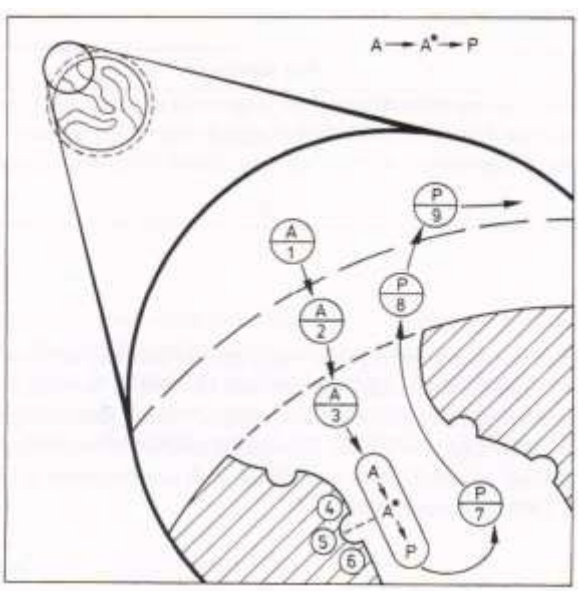

Figure 2-1 Schematic overview of heterogeneous catalysis [39]

$$J_i = -D\frac{\partial c_i}{\partial x} \qquad (5)$$

Here D is the diffusion coefficient, C_i the concentration in a certain dimension and x the distance. Pore diffusion is represented by step 3 and step 7. Here the reactant travels into

the porous pellet to the location it is adsorbed and reversely desorbed as product. The concentration depends on the size of the pores and the penetration depth of the reactants. For a simple first order reaction A → P, the derivation can be simplified using a tube like pore with length/depth L and an accumulation = in – out + reaction equation giving the concentration inside the pore [15]:

$$\frac{C_{A,ads}}{C_A} = \frac{e^{m(L-x)}+e^{-m(L-x)}}{e^{mL}+e^{-mL}} = \frac{\cosh m(L-x)}{\cosh mL} \tag{6}$$

Here $m = \sqrt{\frac{2k\prime}{Dr}}$, with k as reaction coefficient and r as radius of the pore. mL is also referred to as the Thiele modulus M_T.

The rate of steps 4,5 and 6 during methanol synthesis are characterized by different elementary steps in the reaction. The adsorption probability of one of the reactants on the catalyst depends on the coverage of the catalyst surface, which results in an adsorption term in the rate equation. In case the adsorbed reactants interact with one another, this can be included into the rate expression by the addition of an 'effective' value in the rate constant. The rate of the reaction, step 5, is largely dependent on the process conditions whereas they determine the equilibrium or the driving force of the reaction.

Diffusion limitations are common in heterogeneous catalysis and can be ascribed to pellet size, age and activity of the catalyst and reactivity of the reaction components. However, just as the effectiveness of the catalyst, its restrictions are also affected by the temperature, pressure, space velocity and equilibrium approach among other kinetic parameters. To determine the degree of the diffusion limitation theoretical models can be designed, but the complexity of the reaction will be reflected in the model. The simplest and most effective ways to determine them is to use the Thiele modulus or determine them experimentally by varying the particle size of the catalyst [16]. Diffusion limitations are then described by the effectiveness factor η [15].

$$\eta = \frac{\tanh M_T}{M_T} \tag{7}$$

2.1.2 Catalyst activity

In general, the activity of the catalyst in methanol synthesis is in a way proportional to the area of the metallic copper [17, 18]. The effects of the components have been widely discussed throughout literature. Aluminum oxide is considered to act as a structural promoter and reduces the effect of sintering. The active site and the interaction of copper and zinc oxide however, are still under discussion. Several theories are published on how copper and zinc oxide interact. Klier et al [19] assumed a ZnO matrix with a Cu^+ active center. CO and CO_2 are adsorbed on Cu^+, while the present water keeps the catalyst in an optimal oxidation state. Klier based this theory on synergistic effects seen on the catalyst surface, this however does not explain why copper alone or on another support has the same activity. ICI states that the reduced copper metal surface is partly covered by mobile oxygen atoms and carbon dioxide is adsorbed on 'oxidized' copper. The oxygen acts as a promoter for hydrogen dissociation on copper and is a reactant in the shift reaction. Depending on the syngas ratio, 30-40% of the reduced copper can be covered with adsorbed oxygen. CO_2 first reacts with hydrogen to

form a formate intermediate that is first reduced to methoxy and next to methanol. The active sites are formed from adjacent copper atoms and surface oxide. Oxygen remaining on the catalyst surface can react with CO to form CO_2 which is then turned to methanol or reacts with hydrogen and is adopted into the RWGS reaction [20].

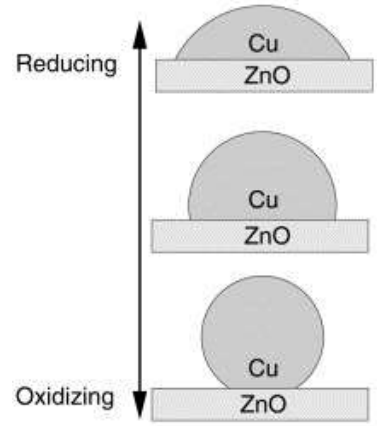

Figure 2-2. Dynamic morphology (wetting/non-wetting effect) of Cu particles on a ZnO support [21]

The Topsøe group explains the promotional role of ZnO in *Cu/ZnO* catalysts by the formation of a CuZn alloy. The zinc oxide stabilizes the higher surface areas for copper crystals and crystal morphologies in a dynamic way depending on the gas composition. The reduction potential of the gas phase dictates whether the copper particles are disk like (reducing) or spherical (oxidizing). The reduction potential is depending or the steam concentration in the gas environment [20, 21] Figure 2-2 shows the dynamic morphology of Cu particles on a ZnO support with changes in the reduction potential. CO_2 is believed to keep the catalysts in an intermediate oxidation state (Cu^0/Cu^+) preventing ZnO reduction [20, 22, 23]. The gas-dependent morphology has been studied using *in situ* using X-ray adsorption fine structure (EXAFS) measurements and were visualized by TEM measurements [20, 21] and is also referred to as wetting/non-wetting behavior. Under reducing conditions a stronger metal surface interaction is found which gives a higher activity. Choi et al. based their theory on the previous, but describe the hydrogenation of both CO and CO_2 over two different active sites. Methanol formation from carbon dioxide proceeds over copper-zinc alloys while the formation of methanol for carbon monoxide is catalyzed by Cu-O-Zn [24, 25].

2.2 Thermodynamics

2.2.1 Chemical equilibria

Gas phase methanol synthesis involves equilibrium reactions as was stated in the introduction. The equilibria of resp. reaction (1), (2) and (3) are expressed as:

$$K_{f_1} = \left(\frac{f_{CH_3OH}}{f_{CO} f_{H_2}^2}\right)_{Eq} = \left(\frac{\varphi_{CH_3OH}}{\varphi_{CO}\varphi_{H_2}^2}\right)_{Eq} \left(\frac{p_{CH_3OH}}{p_{CO} p_{H_2}^2}\right)_{Eq} = K_{\phi_1} K_{p_1} \tag{8}$$

$$K_{f_2} = \left(\frac{f_{CO} f_{H_2O}}{f_{CO_2} f_{H_2}}\right)_{Eq} = \left(\frac{\varphi_{CO}\varphi_{H_2O}}{\varphi_{CO_2}\varphi_{H_2}}\right)_{Eq} \left(\frac{p_{CO} p_{H_2O}}{p_{CO_2} p_{H_2}}\right)_{Eq} = K_{\phi_2} K_{p_2} \tag{9}$$

$$K_{f_3} = K_{f_1} K_{f_2} \tag{10}$$

Here f_i is the fugacity, ϕ_i the fugacity coefficient and p the partial pressure of component i [6]. Fugacity is introduced because water and methanol behave non-ideal at the pressures and temperatures used for synthesis. Because the system is in equilibrium, two reaction equations are sufficient to describe it thermodynamically. Most publications contain experimental results and/or analytical expressions for the equilibrium constants based on thermochemical data described by the ideal gas law together with a correction for non-ideal behavior. The most recent study on the equilibrium values in

methanol synthesis was done by Graaf et al [26]. Graaf used a commercial $Cu/ZnO/Al_2O_3$ catalyst in a range of 1-7 bar and 472-539 K and found that experimental data could be very well described by the ideal gas behavior along with a correction for the non-ideality based on the Soave-Redlich-Kwong equation of state. For pure substances the SRK EOS is as follows;

$$P = \frac{RT}{V-b} - \frac{a(T)}{V(V+b)} \tag{11}$$

Values of terms a and b are calculated using the critical temperatures, critical pressures and acentric factors and are composition dependent in a mixture. For each component the following is used;

$$a_i(T) = a_{c,i}\alpha_i(T) \tag{12}$$

$$b_i = 0.08664\frac{RT_{c,i}}{P_{c,i}} \tag{13}$$

With critical parameter and temperature dependent parameters:

$$a_{c,i} = 0.42747\frac{R^2T_{c,i}^2}{P_{c,i}} \tag{14}$$

$$\alpha_i^{0.5} = 1 + m_i\left(1-\sqrt{T_{R,i}}\right) - p_i\left(1-T_{R,i}\right)\left(0.7-T_{R,i}\right) \tag{15}$$

An additional parameter, the polarity correction parameter p_i, is added to a_i to correct for the presence of polar components and has an empirical value. Parameter m_i is described as follows;

$$m_i = 0.48508 + 1.55191\omega_i - 0.15613\omega_i^2 \tag{16}$$

The SRK can be written in a different format;

$$Z^3 - Z^2 + (A - B - B^2)Z - AB = 0 \tag{17}$$

The fugacity coefficient can be obtained from [26]:

$$ln\,\phi_i = \frac{1}{RT}\int_V^\infty\left[\left(\frac{\partial p}{\partial n_i}\right)_{T,V,n_j} - \frac{RT}{V}\right]dV - ln[Z] \tag{18}$$

This gives the following equation for the fugacity of the vapour phase:

$$ln\,\phi_i^V = \frac{b_i}{b}(Z-1) - ln(Z-B) - \frac{A}{B}\left[\frac{2\sum_{j=1}^n y_j a_{ij}}{a} - \frac{b_i}{b}\right]ln\left(1+\frac{B}{Z}\right) \tag{19}$$

a, a_{ij} and b are respectively given by:

$$a = \sum_{i=1}^n\sum_{j=1}^n y_i y_j a_{ij} \tag{20}$$

$$a_{ij} = \sqrt{a_i a_j}(1 - k_{ij}) \tag{21}$$

$$b = \sum_{i=1}^{n} y_i b_i \tag{22}$$

The fugacity is of component i in the vapour phase is than given by:

$$f_i = y_i \phi_i^V P \tag{23}$$

Most gases show ideal gas behavior at low pressures, it is therefore allowed to assume that at atmospheric pressure $K_f = K_{p^0}$, which is then only dependent on temperature. The value of K_{p^0} can also be derived from temperature, pressure and composition through the following thermodynamic relationship;

$$-\Delta G^0(T) = RT \ln K_{p^0} \tag{24}$$

The specific heats of the components are known to be polynomial functions of T, but can be simplified for small temperature ranges. The following was obtained and used by Graaf et al [26]:

$$log_{10} K_{p_1^0} = \frac{5139}{T} - 12.621 \tag{25}$$

$$log_{10} K_{p_2^0} = \frac{-2073}{T} + 2.029 \tag{26}$$

The system contains polar and non-polar components of which some are above and some below their critical temperatures and pressures. They are listed in Table 1.

Table 1. Critical properties and acentric factors, adopted from [26].

Component	$P_{c,i}$ (bar)	$T_{c,i}$ (K)	$V_{c,i}$ (10^{-6} m^3 mol^{-1})	ω_i
CO	35.0	132.9	93.1	0.049
CO_2	73.8	304.2	94.0	0.255
H_2	20.5	43.6	51.5	0
H_2O	220.5	647.3	56.0	0.344
CH_3OH	81.0	512.6	118.0	0.572

During methanol formation from CO (1) and CO_2 (2) the amount of moles decreases. The amount of moles in the RWGS (3) on the other hand stays the same and makes it independent of the total pressure [27]. Figure 1-4 already showed the equilibria are most favored for methanol synthesis at relative low temperatures and high pressures. The temperature dependence of the equilibria is shown in Figure 2-3. When looking at the plot, the effect of temperature on the K value for the RWGS is limited, meaning its equilibium position is essentially independent of the reaction temperature. The RWGS predominantly takes place on the heterogeneous surfaces of the catalyst and Cu/ZnO based catalysts are known to catalyze the RWGS. The role of this reaction in the Supermethanol region however has to be

investigated as the reaction has an influence on the overall heat balance and concentration of water resulting from the experiments [13] [28].

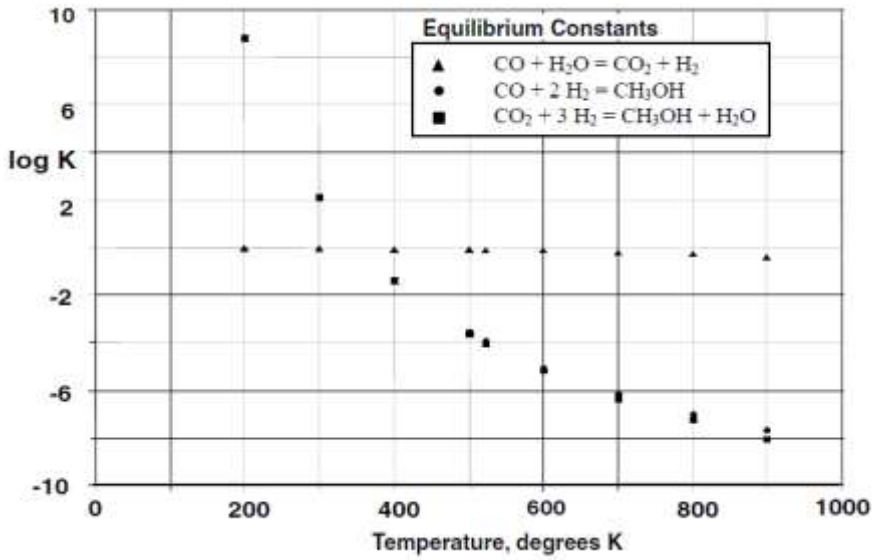

Figure 2-3 Temperature dependence of the equilibrium constants [20]

2.2.2 Syngas composition

In the introduction, the syngas composition ratio has already been mentioned. In order to produce methanol all three components, H_2, CO and CO_2, need to be present in the feed gas. Methanol synthesis over a $Cu/ZnO/Al_2O_3$ catalyst with CO free syngas for instance shows a very slow methanol production that decreases over time. This is explained by the formation of water both from the hydrogenation of carbon dioxide as the RWGS reaction. The buildup of water in the system inhibits the active sites for CO_2 to be transformed to methanol. When CO is considered to be the carbon source, the RWGS reaction has to take place on forehand to provide the component and has to deal with the water inhibiting the catalyst activity. The same decrease in productivity is found for a CO_2 free syngas feed [27].

An overall optimum can be found in syngas composition and productivity when seen from a kinetic point of view. A minimum is found at a composition of 2.5 to 3.5 vol% CO_2, the conversion increases with increasing percentage but makes a quick drop after 12 vol% for industrial conditions [27]. These experiments do not tell anything about the pathway, but set a clear picture that without one of the two, the reaction will not proceed in an optimal way.

2.3 Kinetics

2.3.1 Kinetic models

The kinetic modeling of heterogeneous catalysis depends on the level of understanding of the catalytic reaction. At the most fundamental level, the time development of the system is followed in detail from reactant in a specific quantum state using an equation of motion to the final product. Here, a time dependent Schrödinger equation or Newton's equation is used. When the details of the molecular dynamics are neglected the kinetics can be calculated using a Monte

Carlo approach, which is based on five types of processes taking place; adsorption, dissociation, diffusion, recombination and desorption. For each of the attempted processes the probability of success is taken proportional to the rate [29]. In modeling of the kinetics of methanol however, mostly Langmuir-Hinshelwood models or power law kinetics are used.

2.3.2 Kinetic rate expressions

Several trends have been followed in methanol synthesis over time. The chapter on kinetic expressions also has a long history, an overview of all published kinetic rate expressions for methanol synthesis and the RWGS reaction on copper-zinc catalysts can be found in Methanol Synthesis by Skrzypek et al [30]. To illustrate the background of methanol kinetics a few rate equations are described.

Early kinetic models of methanol synthesis were derived for ZnO/Cr_2O_3 catalysts and high pressure processes. Natta proposed the first kinetic equation in 1955 [7].

$$r_{CH_3OH} = \frac{f_{CO}f_{H_2}^2 - f_{CH_3OH}/K_{eq}^1}{A + Bf_{CO} + Cf_{H_2} + Df_{CH_3OH}} \tag{27}$$

Here f_i is the fugacity of component i and K_{eq} is the thermodynamic equilibrium constant of reaction (1). A, B, C and D are empirical constants depending on temperature and are different for each catalyst. Natta assumed that the hydrogenation of CO was the only reaction occurring and the trimolecular reaction between carbon monoxide and two hydrogen molecules was to be the rate determining step. Bakemeier et al [31] modified the expression of Natta to describe experiments carried out with CO_2 rich feeds. A model with CO_2 dependency followed that used a Langmuir adsorption isotherm. The desorption of methanol was assumed to be rate determining, giving

$$r_{CH_3OH} = \frac{Ae^{-E/RT}\left[P_{CO}^m P_{H_2}^n\left(1-\left(P_{CH_3OH}/P_{CO}P_{H_2}^2K_2^*\right)\right)\right]}{1+De^{-F/RT}P_{CO_2}/P_{H_2}} \tag{28}$$

A, E, m, n, D and F were experimentally determined.

From the 1970's, expressions were based on methanol synthesis over $Cu/ZnO/Al_2O_3$ catalysts. Leonov et al [7] published the first kinetic rate expression of this sort in 1973, however still considering CO to be the only reactant. As mentioned earlier, the group of Klier [19] was the first to acknowledge more reactants. Klier found a maximum in the formation rate while varying the p_{CO}/p_{CO_2} ratio during experiments. The maximum was ascribed to the balance between the promoting effect and strong adsorption of CO_2 on the catalyst surface at high concentrations. Klier used a trimolecular reaction between adsorbed CO and two H_2 molecules to be rate determining in his rate expression and the activity of the catalyst by a redox like mechanism expressed in the equation.

Villa et al [32](1985) included the RWGS in their derivation and published a set of two equations. Even though, the expressions are not very exciting and still based only on reaction (1) and (2), this is the first model that involves more than one active site on the catalyst. The two most recent studies based on reaction (1) and (2) have been done by Askgaard et al and Vanden Bussche and Froment. Askgaard determined the reaction model from surface studies and the

formation of methanol occurs through successive hydrogenation of CO [28]. The reaction from formate to methoxy was appointed to be rate determining. Unfortunately, this model does require lengthy calculations to find the model's parameter and is therefore considered inaccurate. The model of Vanden Bussche and Froment assumes a Langmuir-Hinshelwood/Hougen-Watson mechanism and methanol is formed by successive hydrogenation through formate. The RWGS reaction occurs via a redox reaction [33]

$$r_{CH_3OH} = \frac{K'_{5a}K'_2K_3K_4K_{H_2}p_{CO_2}p_{CH_3OH}\left[1-\frac{(p_{H_2O}p_{CH_3OH})}{(p^3_{H_3}p_{CO_2}K^1_{eq})}\right]}{\left(1+(K_{H_2O}/K_8K_9K_{H_2})(p_{H_2O}/p_{H_2})+(K_{H_2}p_{H_2})^{1/2}+(K_{H_2O}p_{H_2O})\right)^3} \tag{29}$$

$$r_{RWGS} = \frac{K'_1p_{CO_2}\left[1-\frac{(p_{H_2O}p_{CO})}{(p_{CO_2}p_{H_2}K^2_{eq})}\right]}{\left(1+(K_{H_2O}/K_8K_9K_{H_2})(p_{H_2O}/p_{H_2})+(K_{H_2}p_{H_2})^{1/2}+(K_{H_2O}p_{H_2O})\right)} \tag{30}$$

Changing the trend, Skrzypek et al (1991) designed a rate equation assuming CO_2 as carbon source [34]. He also demonstrated experimentally in this study that methanol synthesis from CO is not possible in the absence of water. The model is based on reactions (2) and (3) and uses a Langmuir-Hinshelwood mechanism on the surface of the catalyst with a few intermediate steps. Adsorption of hydrogen and carbon dioxide on the catalyst surface is rate determining in this example, giving the following expressions:

$$r_{CH_3OH} = \frac{k_1K^2_{H_2}K_{CO_2}(P^2_{H_2}P_{CO_2}-(\frac{1}{K^1_{eq}})(\frac{P_{CH_3OH}P_{H_2O}}{P_{H_2}})}{(1+K_{H_2}P_{H_2}+K_{CO_2}P_{CO_2}+K_{CH_3OH}P_{CH_3OH}+K_{H_2O}P_{H_2O}+K_{CO}P_{CO})^3} \tag{31}$$

$$r_{WGS} = \frac{k_2K_{H_2}K_{CO_2}(P_{H_2}P_{CO_2}-(\frac{1}{K^2_{eq}})(P_{CO}P_{H_2O})}{(1+K_{H_2}P_{H_2}+K_{CO_2}P_{CO_2}+K_{CH_3OH}P_{CH_3OH}+K_{H_2O}P_{H_2O}+K_{CO}P_{CO})^3} \tag{32}$$

Graaf et al designed a kinetic model containing all three reactions [35]. Their model is based on a dual-site Langmuir-Hinshelwood mechanism where CO and CO_2 adsorb on site s1 and H_2 and H_2O on site s2. The formation of methanol occurs through successive hydrogenation and the RWGS by a formate mechanism, these are also the rate determining steps for the expressions:

$$r_{CH_3OH,1} = \frac{k_1K_{CO}(f_{CO}f^{3/2}_{H_2}-\frac{f_{CH_3OH}}{f^{1/2}_{H_2}K^1_{eq}})}{(1+K_{CO}f_{CO}+K_{CO_2}f_{CO_2})(f^{1/2}_{H_2}+\left(\frac{K_{H_2O}}{K^{1/2}_{H_2}f_{H_2O}}\right))} \tag{33}$$

$$r_{RWGS} = \frac{k_2K_{CO_2}(f_{CO_2}f_{H_2}-\frac{f_{H_2O}f_{CO}}{K^3_{eq}})}{(1+K_{CO}f_{CO}+K_{CO_2}f_{CO_2})(f^{1/2}_{H_2}+\left(\frac{K_{H_2O}}{K^{1/2}_{H_2}f_{H_2O}}\right))} \tag{34}$$

$$r_{CH_3OH,3} = \frac{k_3 K_{CO_2}\left(f_{CO_2} f_{H_2}^{3/2} - \frac{f_{CH_3OH} f_{H_2O}}{f_{H_2}^{3/2} K_{eq}^2}\right)}{\left(1 + K_{CO} f_{CO} + K_{CO_2} f_{CO_2}\right)\left(f_{H_2}^{1/2} + \left(\frac{K_{H_2O}}{K_{H_2}^{1/2} f_{H_2O}}\right)\right)} \tag{35}$$

The experimental conditions used by the groups described above in determining their rate equation are mostly based on industrial conditions. Overall temperatures are between 400 and 600 K and pressures used are up to 10 MPa [28, 33, 34, 35, 19]. Figure 1-3 already painted the picture of industrial conditions and the large gap between those of the Supermethanol project. With such a variety in expressions for industrial conditions, a rate equation for the Supermethanol project has to be developed to be used as input for designing the optimal reactor configuration.

3 Theory

3.1 Derivation of the kinetic rate expression

As described throughout the previous chapters, methanol can be formed via the highly exothermic hydrogenation of carbon monoxide or carbon dioxide and carbon dioxide can be converted via the RWGS. The first two reactions are exothermic and all three are equilibrium limited. In developing a kinetic model the Supermethanol project both the hydrogenation of CO as CO_2 are incorporated in the model [35]. The RWGS reaction is normally very slow but can be promoted by copper containing catalysts [36]. Even though its role is expected to be small, the RWGS has an influence on the reaction systems components and the overall heat balance and is therefore also incorporated in the derivation of the kinetic models.

3.1.1 Langmuir-Hinshelwood/Hougen-Watson

Based on the level of understanding of the catalytic process, differently detailed models can be chosen to describe the kinetics. A Langmuir-Hinshelwood/Hougen-Watson mechanism was chosen to be the basis for the first model, as is the most commonly used model in methanol kinetics [32, 35]. The rate expression of a Langmuir-Hinshelwood/Hougen-Watson mechanism looks as follows:

$$r = \frac{(kinetic\ factor)\cdot(driving\ force)}{(adsorption\ term)^n} \tag{36}$$

The kinetic factor contains the relevant rate coefficients being the catalyst activity, surface reaction rate and number of catalyst active sites. The driving force is based on one of the elementary reaction that is considered rate controlling and the adsorption term describes the availability of the active sites, in which the power n of the absorption term represents the number of catalytic involved in the molecular reaction. The adsorption term has a general form of:

$$(1 + K_a p_a + K_b p_b + \cdots)^n \tag{37}$$

Each term is proportional to the surface coverage of the respective species; they are scaled so that the '1' is proportional to the vacant surface [37].

This model is based on the kinetic model of Graaf [35] and also contains three equations each describing one of the three equilibrium reactions. Here, the kinetic factor is described by one rate constant, k_i, which includes the catalyst activity, surface reaction rate and number of catalyst active sites per weight of catalyst. The kinetic factor is obtained from the experimental data and should always be > 0. The driving forces used in Graaf's research resulted from elementary reactions and two active sites on the catalyst. Instead of using the elementary reactions, the first estimations are made using the overall formation reactions. Furthermore, as methanol synthesis takes place in a gaseous system containing polar and non-polar components, fugacity's of the reaction components are used in describing the driving forces and chemical equilibrium constant, $K_{p_i^0}$, instead of partial pressures.

The adsorption term is based on a catalyst containing two active sites. On catalytic site one, s1, CO and CO_2 adsorb competitively. On catalytic site two, s2, H_2 and H_2O adsorb competitively, hydrogen is believed to adsorb dissociative

and the term is for that reason written as a square root [35]. For this model, the total number of sites, s1 and s2, is regarded constant per weight of catalyst. As reaction (1), (2) and (3) all involve catalytic sites s1 and s2, the adsorption term is identical in all three equations. Due to the rapid progress of the reaction, adsorption and desorption steps are not considered to be rate determining, methanol is therefore not present in the adsorption term. Water on the other hand could cause an inhibiting effect on the production rate and is therefore present in the adsorption term. A table containing the adsorption equilibria, elementary reactions and driving forces used in the derivation of the model is added to Appendix 9.1 as developed by Graaf [35]. The kinetic model is shown below:

$$r_1' = \frac{k_1\left(f_{CO} f_{H_2}^2 - \frac{f_{CH_3OH}}{K_{p_1^0}}\right)}{\left(1+K_{CO} f_{CO}+K_{CO_2} f_{CO_2}\right)^n \left(1+K_{H_2}^{1/2} f_{H_2}^{1/2}+K_{H_2O} f_{H_2O}\right)^n} \tag{38}$$

$$r_2' = \frac{k_2\left(f_{CO_2} f_{H_2} - \frac{f_{H_2O} f_{CO}}{K_{p_2^0}}\right)}{\left(1+K_{CO} f_{CO}+K_{CO_2} f_{CO_2}\right)^n \left(1+K_{H_2}^{1/2} f_{H_2}^{1/2}+K_{H_2O} f_{H_2O}\right)^n} \tag{39}$$

$$r_3' = \frac{k_3\left(f_{CO_2} f_{H_2}^3 - \frac{f_{CH_3OH} f_{H_2O}}{K_{p_3^0}}\right)}{\left(1+K_{CO} f_{CO}+K_{CO_2} f_{CO_2}\right)^n \left(1+K_{H_2}^{1/2} f_{H_2}^{1/2}+K_{H_2O} f_{H_2O}\right)^n} \tag{40}$$

The fugacity's are obtained from experimental data, using a modification of the SRK equation of state as was described in the previous chapter [26]. For the equilibrium $K_{p_1^0}$ and $K_{p_2^0}$ values, equation (8) and (9) are used which were also introduced in the previous chapter [26]. Because reaction (3) is the stoichiometric sum of reaction (1) and (2), the chemical equilibrium constant for reaction (3) can be written as;

$$K_{p_3^0} = K_{p_1^0} K_{p_2^0} \tag{10}$$

3.1.2 Power law model

When less is known about the reaction mechanism, a power law can be used to describe the system. The chosen power law looks a follows:

$$r_1' = A_1 e^{E_{a,1}/RT} f_{H_2}^{l_1} f_{CO}^{l_2} \left(\xi - f_{CH_3OH}\right)^{l_3} \left(1 - \frac{f_{CH_3OH}}{f_{CO} f_{H_2}^2 K_{p_1^0}}\right) \tag{41}$$

$$r_2' = A_2 e^{E_{a,2}/RT} f_{H_2}^{m_1} f_{CO_2}^{m_2} \left(\xi - f_{H_2O}\right)^{m_3} f_{CO}^{m_4} \left(1 - \frac{K_{p_2^0} f_{H_2O} f_{CO}}{f_{CO_2} f_{H_2}}\right) \tag{42}$$

$$r_3' = A_3 e^{E_{a,3}/RT} f_{H_2}^{n_1} f_{CO_2}^{n_2} \left(\xi - f_{H_2O}\right)^{n_3} \left(\xi - f_{CH_3OH}\right)^{n_4} \left(1 - \frac{f_{CH_3OH} f_{H_2O}}{f_{CO_2} f_{H_2}^3 K_{p_3^0}}\right) \tag{43}$$

The equation contains an Arrherius constant, A, activation energy term, E_A, the partial fugacity's of the reactants and products and the driving force. The ξ term is introduced to account for possible inhibiting effect by one of the formed products. The fugacity's are obtained from experimental data, l_i, m_i and n_i represent their orders, respectively. The

chemical equilibrium is accounted for in the last term, here equilibrium values $K_{p_1^0}$ $K_{p_2^0}$ and $K_{p_3^0}$ are calculated as described above by using the equations from Graaf et al. [26].

3.2 Parameter estimation

From the experiments production rates of methanol and water, respectively R'_{CH_3OH} and R'_{H_2O}, are obtained at varying reaction temperatures and pressures and varying feed gas compositions at different volumetric flows. The theoretical production rates for methanol and water were fitted to the experimental data. The parameters need to be estimated, which is done by using Matlab function 'lsqcurvefit' to fit the kinetic model to the experimental data.

The predicted production rates of methanol are described as follows:

$$\hat{R}'_{CH_3OH} = r'_1 + r'_3 \tag{44}$$

$$\hat{R}'_{H_2O} = r'_2 + r'_3 \tag{45}$$

To find the best fitting parameters the sum of squared residuals method (SSR) was used, using the total predicted and experimental total production rates of methanol and water:

$$SSR = \sum_{l=1}^{N} \left(\left(\hat{R}'_{CH_3OH} - R'_{CH_3OH} \right)_l^2 + WF \left(\hat{R}'_{H_3O} - R'_{H_2O} \right)_l^2 \right) \tag{46}$$

N is the number of experiments for every fitted parameter and WF is representing the weighing factor. The WF is equal to 1 when the estimated water production rate is valued equal to that of methanol. With WF equal to 0, the estimated water formation rate is not included in the parameter estimation. The SSR should be normally distributed with a zero mean and the residuals should show no trending effects as a function of any of the independent variables. The values of the variances are composed of lack of fit of the model together with experimental errors, a standard function of Matlab was used. Average absolute errors in the experiments are calculated using:

$$\Delta R'_i = \frac{1}{N} \sum_{i=1}^{N} \left| \frac{\hat{R}'_i - R'_i}{R'_i} \right| \cdot 100\% \tag{47}$$

All Matlab codes used in the parameter estimation can be found in Appendix 9.3.

4 Experimental

4.1 Materials

Pure gases used for the experiments (CO > 99.955 vol%, CO_2 > 99.7 vol%, H_2 > 99.999 vol%) were supplied by Linde Gas Benelux, The Netherlands. The average gas compositions used in the kinetic experiments can be found in Table 2. The nitrogen concentration was below 0.5 vol% for the experiments used for the derivation of the kinetic models and is neglected. The gas mixtures used for the kinetic experiments with predetermined compositions, were tailor made in the setup (Figure 4-2) using a gas mixing station, which induced some fluctuations in the feed gas composition (± 2.5%). For the determination of the kinetics a commercial Cs doped $Cu/ZnO/Al_2O_3$ methanol synthesis catalyst was used in powder form with a mean diameter of 0.25 to 0.43 mm for all experiments.

Table 2. Average gas composition used for the kinetic experiments.

Composition	H_2 (vol%)	CO (vol%)	CO_2 (vol%)	P (MPa)	T (K)	$\Phi_{V,\,in}$ (NL/min)	S_N
1	69.4	27.5	3.1	17.5-22.5	483-498	0.5-1.0	2.2
2	63.5	23.1	13.4	17.5-22.5	483-498	0.5-1.0	1.4
3	74.9	18.4	6.6	17.5-22.5	483-498	0.5-1.0	2.7
4	80.2	10.4	9.3	17.5-22.5	483-498	0.5-1.0	3.6
5	89.6	4.8	5.6	17.5-22.5	483-498	0.5-1.0	8.1
6	84.4	13.1	2.5	17.5-22.5	483-498	0.5-1.0	5.3
7	86.4	1.2	12.4	17.5-22.5	483-498	0.5-1.0	5.4

4.2 Experimental setup

A schematic overview of the mixing station and experimental setup used in the kinetic experiments is shown in Figure 4-2. The pure gases used for the gas mixtures are connected to the gas mixing station and by adjusting the mass flow controllers (MFC, Brooks Instruments) the desired composition is obtained. The gas mixture is collected in a gas storage vessel (V = 0.5 L) and pressurized in a gas booster (Resato, High pressure technology) to approximately 30 MPa and stored in a gas bomb (V = 1 L). A set mass flow is fed to the spinning basket reactor by another adjustable MFC (Brooks Instruments). To keep a constant feed flow to the reactor, new syngas is prepared concurrent with the experiments using the gas mixing system.

A Rushton turbine was used to stir the reactor with a rotating speed to be adjusted from 0 to 2500 rpm. Attached to the rotor is a basket containing the catalyst particles (0.1 – 0.3 g), both the spinning basket and propeller are shown in Figure 4-1. The volume of the reactor is reduced to 50 mL by an inert stainless steel block. The gas is fed to the reactor from the top and is forced down through the spinning basket containing the catalyst. The spinning basket reactor is electrically heated and the temperature is controlled by a thermocouple located close to the spinning basket. The gas mixture leaves the reactor from the bottom through a dip tube. The pressure in the reactor is controlled with a back-pressure valve

(BPV) (Swagelok, which was later replaced by a BPV from Equilibar). The outlet stream of the reactor was traced (dotted line) and kept at a temperature of 393-403 K to prevent condensation in the tubes. Part of the reactor effluent is fed to a gas chromatograph (GC). The composition of the gas flow is directly analyzed in the GC. The remaining gas stream and the GC effluent are quantified using a wet gas-meter. This method is used during the kinetic experiments. A bypass around the reactor to the GC is used to obtain the composition of the feed. In blank runs with no catalyst at elevated temperatures the composition of the feed was equal to the composition of the off gas confirming the inertness of the system with no catalyst present.

Figure 4-1 Spinning basket used during the kinetic experiments.

The MFC controlling the feed to the reactor, a pressure indicator and a temperature indicator on the reactor and an additional temperature indicator on the effluent gas tube are connected to a Virtual Bench Logger system for means of monitoring the experiments.

4.3 Analyses

The gas composition was analyzed using an online Compact GC (Interscience) with thermal conductivity detectors. Helium was used as a carrier gas. H_2, CH_4 and CO are analyzed on a molecular sieves 5 Å column (L = 5 m), CO_2, H_2O and CH_3OH are analyzed on a Porabond Q column (L = 10 m). The GC was calibrated with premixed and syngas supplied en certified by Linde Gas Benelux, (CO_2 = 10.6 vol%, CH_4 = 10.1 vol%, CO = 24.0 vol%, H_2 = 55.3 vol%). The calibration for H_2O and CH_3OH was done using a saturated N_2 stream with either one of the components. Six wash bottles containing methanol or water were connected in series through which the N_2 stream was bubbled. To ensure the stream was saturated, several flowrates were used during the calibration. Obtaining constant values was found to be more difficult for the calibration of water and therefore a larger error in the water GC data should be taken into account when discussing the results.

4.4 Measurements

The reaction temperature was measured as close as possible to the spinning basket, fluctuations were below 0.6 K from the average temperature for all experiments. The temperature and pressure were logged. An additional local pressure gauge was used as safeguard for the pressure in the reactor. The gas composition was analyzed every 90 s. Measurements were considered steady state after five times the residence time and at least 10 minutes of more or less constant concentrations (slightly decreasing or increasing concentrations were accepted) and stable measurements (no methanol spikes due to condensation).

For the kinetic measurements approximately 0.1 – 0.3 g of catalyst was used. Every day a fresh batch of catalyst was activated with H_2 overnight according to the following program (2 h at 443 K, 2 h at 473 K, 2 h at 493 K, 3 Nm^3/kg cat./h, 0.2 MPa). The maximum operating time of one batch of catalyst was 12 h. After every experimental set the system was flushed with nitrogen and cooled down under nitrogen atmosphere.

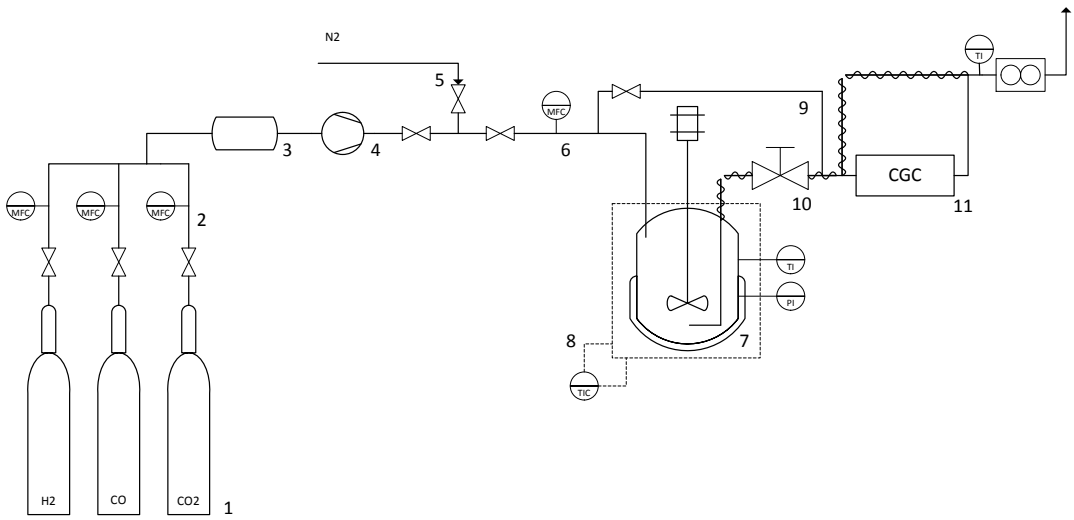

Figure 4-2. Flow scheme of the equipment used for the kinetic experiments.1 gas cylinders; 2 mass flow controllers and control device; 3 booster; 4 nitrogen in-flow; 5 hydrogen in-flow; 6 mass flow controller; 7 spinning basket reactor; 8 thermostat; 9 by-pass; 10 back-pressure valve; 11 CGC; 12 wet gas meter; dotted line represents the tracer.

4.4.1 Measurements of production rates

The spinning basket reactor is assumed to be a perfectly mixed CISTR. The rates of methanol and water formation were calculated from the following mixed flow material balances over the reactor.

$$R'_{CH_3OH} = y_{CH_3OH} \frac{\phi_{V,off}}{W} \frac{P}{RT} \qquad \text{(mol/g cat./h)} \qquad (48)$$

$$R'_{H_2O} = y_{H_2O} \frac{\phi_{V,off}}{W} \frac{P}{RT} \qquad \text{(mol/g cat./h)} \qquad (49)$$

Here, R'_i is the rate of formation of methanol or water, y_i the methanol or water mole fraction, $\phi_{V,off}$ the volumetric flow rate of the exit gas, W the catalyst weight, P the pressure of the exit gas flow, R the universal gas constant and T the temperature of the exit gas flow.

5 Results and discussion

5.1 Diffusion limitations and catalyst deactivation

Before starting the kinetic experiments, measurements were done to assess the effect of diffusion and heat transfer limitations on the overall reaction rates. The method used to determine external and internal mass and heat transfer limitations, was introduced by Brown and Bennet [16]. Internal mass and heat limitations were investigated using four different particle diameters (0.25-0.43 mm, 0.8 – 1.0 mm, 2.5-2.8 mm and pellet size of approximately 5 mm). The experiments were conducted at 498 K and 523 K and 20.0 MPa. The results of the experiment done at 523 K are shown in Figure 5.1a. The values for the three smallest particle sizes are comparable and it is therefore assumed that internal mass transfer limitations are not present. The catalyst particles used in the kinetic experiments have a diameter of 0.25-0.43 mm.

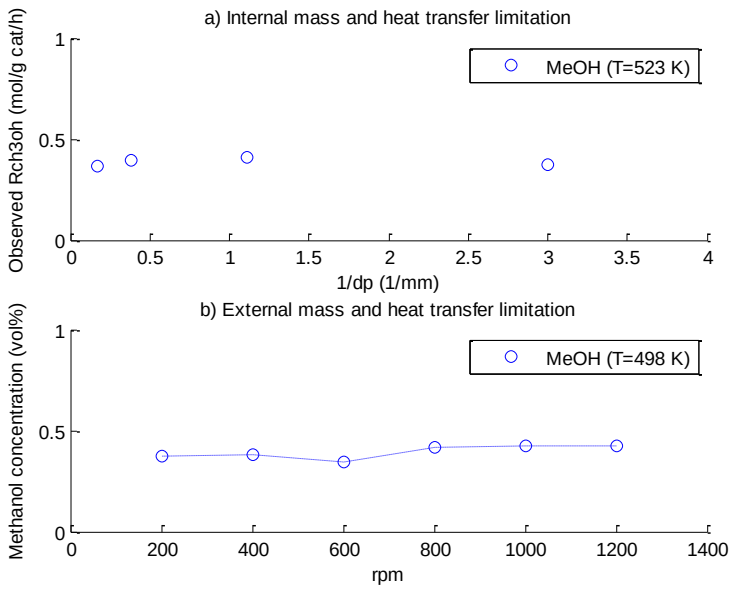

Figure 5-1 a) Methanol production rate as a function of the particle size. P = 20.0 MPa, T = 523 K syngas H2/CO/CO2 = 70.3/25.4/4.3 vol%. b) Methanol concentration in effluent stream as function of rotational speed P = 20.0 MPa, T = 498 K, syngas H2/CO/CO2 = 74.7/20.3/5.0 vol%.

External mass and heat transfer limitations were investigated using catalyst particles of 0.25-0.43 mm and varying rotational speed of the spinning basket. The experiments were done with 0.5 grams of catalyst, a temperature of 498 K, a pressure of 20.0 MPa and an ingoing flow rate of 30 NL/h, the results are shown in Figure 5-1b. The methanol concentration in the effluent gas of the reactor does not seem to be influenced by rotational speed of the catalyst containing basket on the rotor. It was therefore assumed that the external mass and heat transfer limitations are negligible in this system. This method of evaluation was found and proven to be more reliable than calculating the mass transfer coefficient based on circular rotations of the spinning basket by Brown and Bennet [16]. A speed of 1500 RPM was used for all experiments.

Throughout the kinetic measurements, a fresh batch of catalyst was used daily which had been reduced overnight. To check if catalyst deactivation occurred over the course of the experiment, a twelve hour experiment was conducted. The results are shown in Figure 5-2. At t=0 the reactor was 498 K the syngas feed started and the pressure was slowly increased to 20.0 MPa. The effluent concentration slightly increased in the first two hours but then appears stable throughout the experiment. Based on this result the deactivation of the catalyst is assumed to be negligible. Even though there were fluctuations in the feed gas composition during the experiment, the formation rate of methanol remained stable. During the kinetic experiments these fluctuations are neglected.

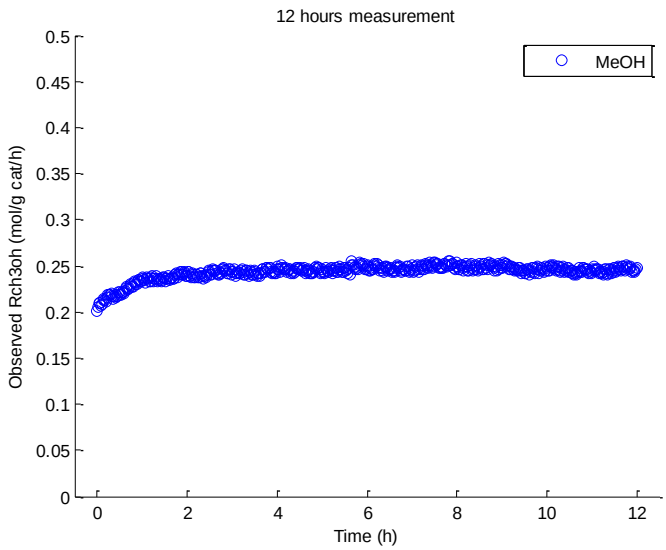

Figure 5-2. Methanol production rate in the effluent stream as function of on-stream time (mol/g cat/h). P = 20.0, T = 498 K, syngas H2/CO/CO2 = 68.3/27.6/4.1 vol%.

During consecutive experiments in which the temperature was lowered the methanol formation rate was found not to decrease with the decreasing temperature when cooled under syngas conditions. This was probably caused by the fast exothermic formation reactions, leading to a higher than anticipated temperature of the catalyst. To ensure that this phenomenon did not affect the catalyst activity or other experiments, the reactor was cooled down under nitrogen conditions and sometimes a check-up experiment was conducted. An additional experiment was done where the catalyst particles were mixed with inert grid to ensure the absence of a temperature gradient in the reactor.

5.2 Production rates of methanol and water

The experiments were carried out at three different pressures, using three different flow rates. Figure 5-3. a) shows the methanol formation rates plotted against reaction pressure for syngas feed 2. Typical of methanol synthesis is that production rates for methanol synthesis increase with increased partial pressure, which is seen in the plot. This is also the typical in methanol synthesis under industrial conditions (to approximately 10 MPa) and the expected trend for the Supermethanol experiments.

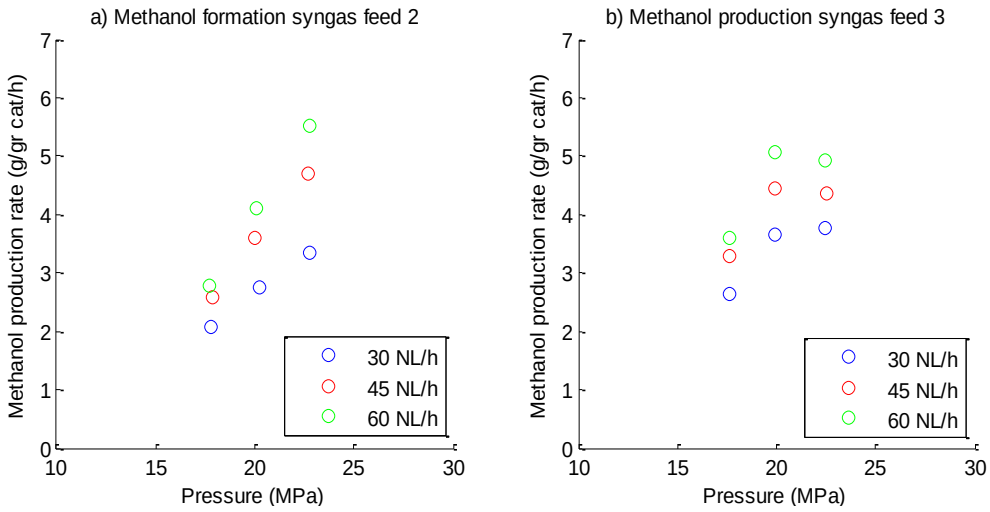

Figure 5-3 Methanol concentration in the effluent stream as a function of pressure at T = 483 K, a) syngas feed 2 H2/CO/CO2 = 63.5/23.1/13.4 vol%, Sn = 1.4. b) syngas feed 3 H2/CO/CO2 = 74.9/18.4/6.6 vol%, Sn = 2.7.

Figure 5-3. b) shows the trend of the methanol production rate of syngas feed 3. Most of the data obtained in the experiments resembles the trend shown, instead of increasing production rates, the production rates of the experiments done on 20 and 22.5 Mpa look rather similar. This could indicate that in the pressure range of the Supermethanol project, the rate of formation is no longer positively influenced by pressure in all cases. The production rates in Figure 5-3. b) can also be interpreted as slightly decreasing at 22.5 MPa, which could point to the adsorption of one of the components onto the catalyst causing an inhibiting effect on one or more of the reactions. Figure 5-4 a) and b) show the water production rates of water belonging to the experiments just discussed. The trends here both do not indicate a dependence on pressure. What's interesting is the rate of which water is formed for the two different feed gases. Figure 5-4 a) shows a different trend for water production than was measured for methanol in Figure 5-3 a) showing that in this

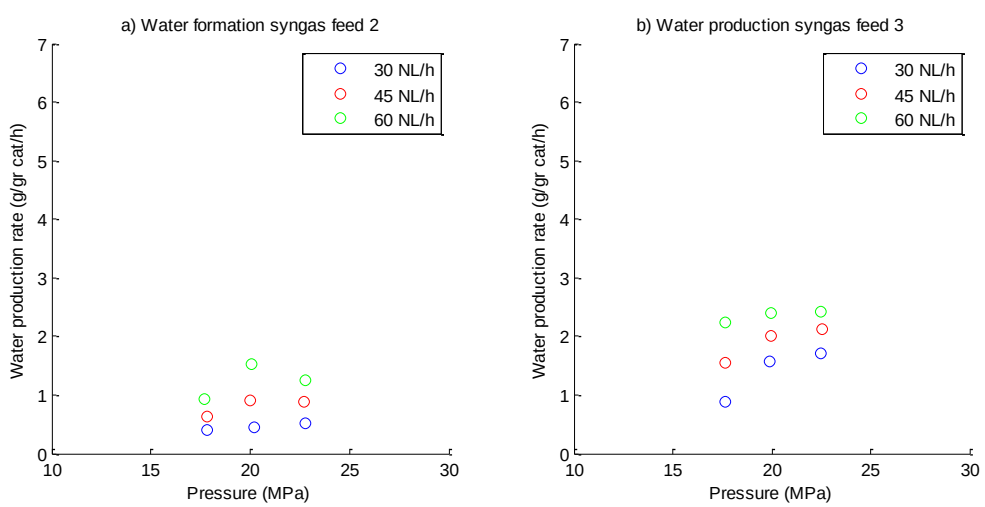

Figure 5-4 Methanol concentration in the effluent stream as a function of pressure at T = 483 K, a) syngas feed 2 H2/CO/CO2 = 63.5/23.1/13.4 vol%, Sn = 1.4. b) syngas feed 3 H2/CO/CO2 = 74.9/18.4/6.6 vol%, Sn = 2.7.

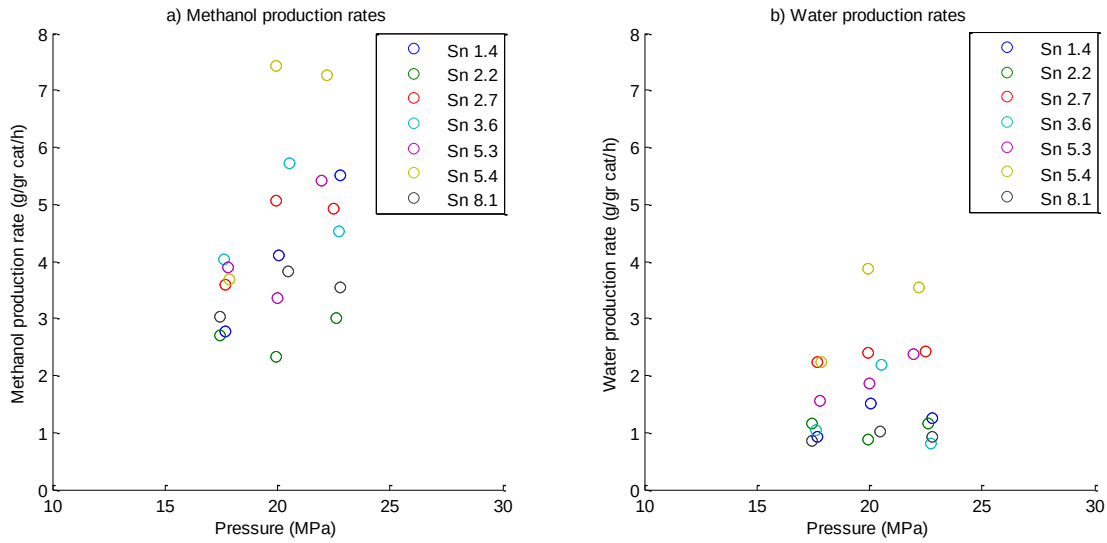

Figure 5-5 a) Methanol and b) water production rates according to their S_N value

case the increased pressure does not increase the production rate of methanol from CO_2. The production rate of water in Figure 5-4 b) is higher, showing that with this feed gas composition, CO_2 is more often the carbon source for methanol. When looking at the components ratios of the feed, syngas feed 2 has an S_n value of 1.4 with high amounts of CO to CO_2 and hydrogen as the limiting component. Syngas feed 3 has an S_n value of 2.7, meaning CO and CO_2 are the limiting components. It is likely that the composition of the feed gas has an influence on the reaction rate. In Figure 5-5 the production rates for the different feed gases at T =483 K and ϕ_V = 60 NL/h are plotted. Even though the plot is rather chaotic some trends are clear. The lowest reaction rate for both methanol and water, is found for syngas feed 1 which has S_N value 2.2. This is interesting as this is the standard composition used in industry. The largest production rates for methanol and water formation originate from experiments using syngas feed 7 with S_N value 5.4, which is the

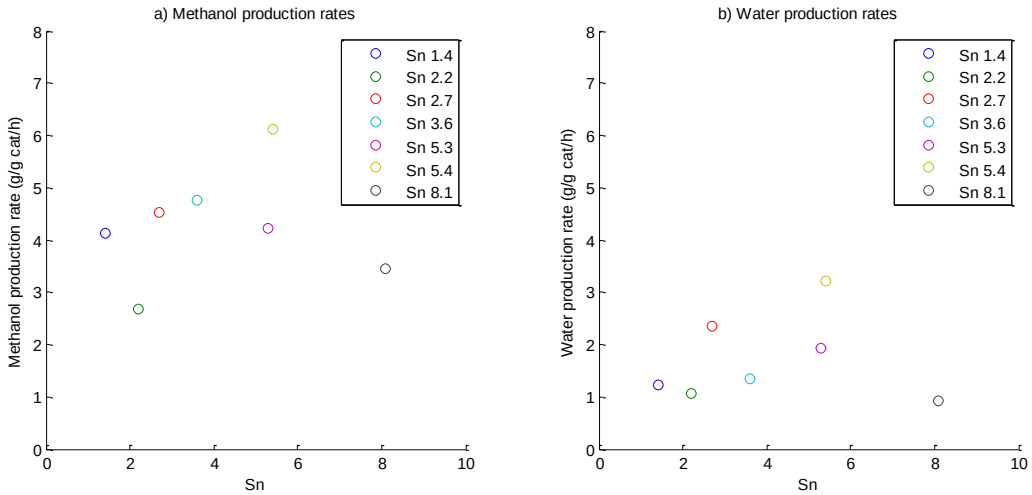

Figure 5-6 a) Methanol and b) water production rates according to their S_N value

feed gas containing much more CO_2 than CO. If we assume CO_2 to be the carbon source for methanol, the faster production rate is simply explained by the amount of CO_2 available to the catalyst. The same trends are seen for the production rates of water. As we expect the WGS to be a slow reaction, the reaction rate of water formation can be directly linked to the percentage of methanol formed from CO or CO_2. When we plot the average production rates against their S_N value, we unfortunately don´t see an immediate trend. However, the plot in Figure 5-5 shows the highest production rates in the Supermethanol region are not found around S_N 2 as earlier established for medium pressure reactions, but between S_N values between 2.5 and 6.

5.3 Parameter estimation

5.3.1 Parameter estimation LHHW model

The experimental gave 192 datasets to be used in the derivation of the model with variations in temperature, pressure, flow rate and feed composition. 142 datasets were used in the initial parameter estimation. The parameters were estimated using Matlab function 'lsqcurvefit' and the sum of squared residuals method to find the best fitting parameters. After the first fitting exercise, the dataset showing an average error over 100% for methanol were excluded from the estimation data. Finally 126 datasets remained which can be considered to be an experimental dataset obtained at 483 K and a second experimental dataset obtained at 498 K. During the second parameter fitting, the value of the adsorption constant for water, K_{H_2O}, was found to tend to zero and could be excluded from the adsorption term. The term for adsorption describes the surface coverage of the catalyst, where the adsorbed components are proportional to the unoccupied active sites. Now, eight parameters remain to be estimated. The best fitting parameters were found using the experimental data that were obtained at 483 K giving the lowest SSR and smallest standard deviation. The best fitting parameters are shown in Table 3 and give the following kinetic equations;

Table 3 Values for the fitted parameters of the LHHW based kinetic model

Parameter	Value	Kinetic model
k_1	0.1025	
k_2	$1.00*10^{-6}$	$r_1' = \frac{0.1025\,(f_{CO}f_{H_2}^2 - \frac{f_{CH_3OH}}{K_{p_1^0}})}{(1+1.693f_{CO}+1.794f_{CO_2})^{1.807}(1+1.4887f_{H_2})^{1.292}}$ (47)
k_3	0.2430	
K_{H_2}	1.488	$r_2' = \frac{1.0*10^{-6}(f_{CO_2}f_{H_2} - \frac{f_{H_2O}f_{CO}}{K_{p_2^0}})}{(1+1.693f_{CO}+1.794f_{CO_2})^{1.807}(1+1.4887f_{H_2})^{1.292}}$ (48)
K_{CO}	1.693	
K_{CO_2}	1.794	$r_3' = \frac{0.2430\,((f_{CO_2}f_{H_2}^3 - \frac{f_{CH_3OH}f_{H_2O}}{K_{p_3^0}})}{(1+1.693f_{CO}+1.794f_{CO_2})^{1.807}(1+1.4887f_{H_2})^{1.292}}$ (49)
n_1	1.807	
n_2	1.292	

The first thing to be noticed on this model is the values of the kinetic terms. The two methanol production rates (47) and (49) are of the same magnitude and the production rate of the RWGS (48) is much smaller, indicating that the RWGS plays only a minor role in the reaction system. The second noticeable values, are those of the estimated orders in the adsorption term. The estimated values of n_1 and n_2 are found to be respectively 1.807 and 1.292, but were expected to both have a value of 1. This means that a total of three active sites would be involved in the formation reaction. Overall, the values found in the parameter estimation do not resemble an extension of the model developed by Graaf, on which the model is based. When looking at other previously published models, a publication by Skryzepek [34] describes a kinetic model with an overall third order adsorption term. His model however is based on formation reactions (2) and (3) and a catalytic mechanism with one type of active site and not two as was done by Graaf. Vanden Bussche and Froment [33] also have a third order for the denominator in their methanol equation, they too assume a single type of active sites and base their model on reaction (2) and (3). In both these models the three sites are occupied by the molecules of the rate determining step, but based on a different reaction mechanism.

The results of the estimation are made visible in a parity plot for methanol and water production as shown in Figure 5-7 where the predicted and observed production rate is plotted against one another. The blue dots represent the values for methanol at temperature T = 483 K, and shows an average relative error $\Delta R'_{CH_3OH}$ of 69.7 %. The predicted and observed values for water are represented by the blue stars in the parity plot on the right. Here an average relative error $\Delta R'_{H_2O}$ of 101.5% is found. Including the experimental data obtained at 498 K increased the average error of the model for $\Delta R'_{CH_3OH}$ to 71.7 % , and for water to $\Delta R'_{H_2O}$ 139.4 %.

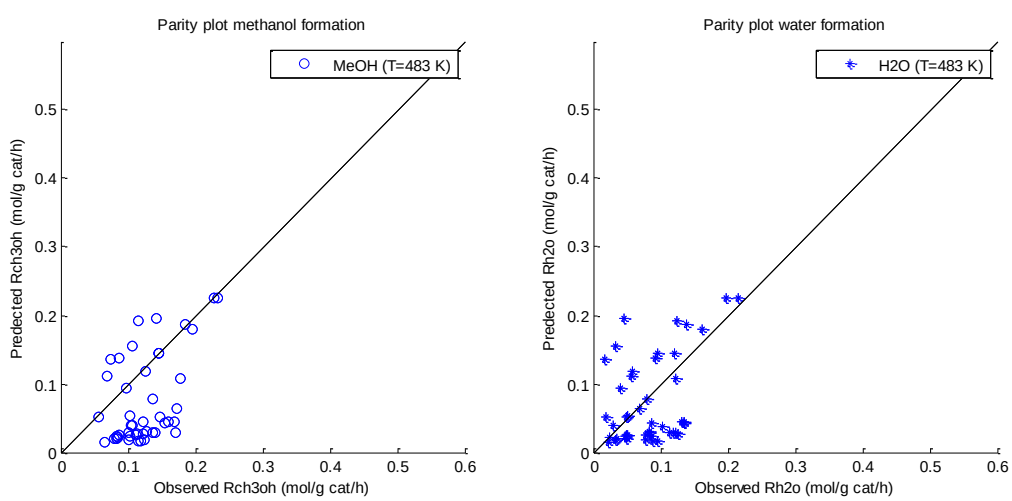

Figure 5-7 Parity plot of the LHHW model showing the predicted against the observed production rates of the kinetic experiments for methanol and water formation at T = 483 K.

The experimental data cannot be accurately described by this simplification of the LHHW model, the model is therefore dismissed. The reason for this is not clear, but the limited dataset, experimental error or product condensation, and

inaccuracy of the GC due to its calibration might be factors playing a role. Or as the reaction mechanism is not clear a model using the wrong terms was chosen.

5.3.2 Power law model

A simpler kinetic power law model incorporating all three reactions, introduced in chapter 3, was used to fit the obtained data. The first estimation included only the data obtained at 483 K and the temperature dependent factor was replaced by k_i, the inhibition terms were removed from the equation to limit the number of freely varying parameters. The fugacity's are obtained from experimental data, and l_i, m_i and n_i represent their orders, respectively. The equilibrium values $K_{p_1^0}$ $K_{p_2^0}$ and $K_{p_3^0}$ are calculated using the equations from Graaf et al. [26]. The parameter estimation was done using the 'lsqcurvefit' function in Matlab. Datasets with an average error over 40% for methanol were removed from the dataset in the next estimation. The parity plot of the estimation is shown in Figure 5-8 giving an average absolute error of 19.2 % for methanol and 47.3 % for water. The estimated reaction orders for the fugacity terms of methanol, water and carbon monoxide in the RWGS reaction tended towards zero and were therefore omitted, reducing the total number of

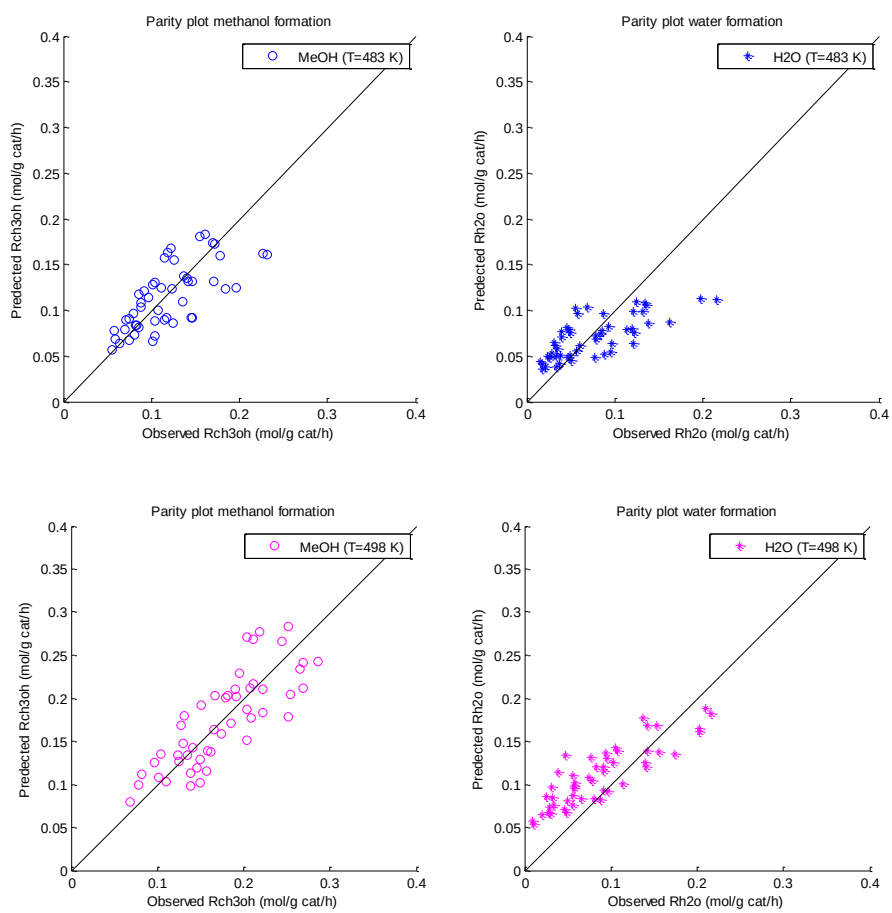

Figure 5-8. Parity plot of the power law model showing the predicted against the observed production rates of the kinetic experiments for methanol and water formation at a)T = 483 and b) T = 498 K.

parameters to 8. The same was done for the datasets obtained at 498 K, giving an average error for methanol of 16.6% and for water of 77.6%. The parity plot belonging to this estimation is shown in Figure 5-8. The estimated parameters are tabulated in Table 5. The parity plots give a good indication on the accuracy of the parameter estimation, in both cases the dots are spaced around the diagonal for the methanol estimation. As the estimation was largely influenced by the influence of methanol by means of the WF, the parity plot of the water formation is less accurate.

Table 4 Values for the fitted parameters of the power law model.

Dataset 483 K		Dataset 498 K		
Parameter	**Value**	**Parameter**	**Value**	
k_{r1}	0.7881	k_{r1}	0.7190	
k_{r2}	0.8889	k_{r2}	1.2191	$r_1' = k_1 f_{H_2}^{l_1} f_{CO}^{l_2}\left(1 - \frac{f_{CH_3OH}}{f_{CO} f_{H_2}^2 K_{p_1^0}}\right)$ (50)
k_{r3}	0.2624	k_{r3}	0.2054	
l_{H_2}	0.0459	l_{H_2}	0.0246	
l_{CO}	0.1112	l_{CO}	0.2375	$r_2' = k_2 f_{H_2}^{m_1} f_{CO_2}^{m_2}\left(1 - \frac{K_{p_2^0} f_{H_2O} f_{CO}}{f_{CO_2} f_{H_2}}\right)$ (51)
m_{H_2}	0.0363	m_{H_2}	0.0263	
m_{CO_2}	0.1152	m_{CO_2}	0.2168	
n_{H_2}	0.0268	n_{H_2}	0.0107	$r_3' = k_3 f_{H_2}^{n_1}\left(1 - \frac{f_{CH_3OH} f_{H_2O}}{f_{CO_2} f_{H_2}^3 K_{p_3^0}}\right)$ (52)
$\Delta R'_{CH_3OH}$	19.2	$\Delta R'_{CH_3OH}$	16.6	
$\Delta R'_{H_2O}$	47.3	$\Delta R'_{H_2O}$	77.6	

As the estimated parameters for these two power laws are of comparable size, an isotherm was added to the model and estimation was done with both sets. The constant k_i was replaced with $A_i \exp(E_a/RT)$ containing the Arrhenius constant, A, activation energy term, E_A, the gas constant R and reaction temperature T making the model temperature dependent. The relative average error was found to be $\Delta R'_{CH_3OH}$= 23.7 % for methanol and $\Delta R'_{H_2O}$ = 43.2 % for water. The model and the estimated parameters are shown in Table 5.

Table 5 Values for the fitted parameters of the power law based kinetic model

Parameter	Value	Kinetic model
A_{r1}	0.7897	
A_{r2}	0.1077	
A_{r3}	0.8939	$r_1' = 0.7897 e^{-230.6/RT} f_{H_2}^{0.1054} f_{CO}^{0.2580}\left(1 - \frac{f_{CH_3OH}}{f_{CO} f_{H_2}^2 K_{p_1^0}}\right)$ (53)
$E_{a,r1}$	-230.6	
$E_{a,r2}$	-133.3	
$E_{a,r3}$	-180.8	$r_2' = 0.1077 e^{-133.2/RT} f_{H_2}^{0.0225}\left(1 - \frac{K_{p_2^0} f_{H_2O} f_{CO}}{f_{CO_2} f_{H_2}}\right)$ (54)
l_{H_2}	0.1054	
l_{CO}	0.2580	
m_{H_2}	0.0225	$r_3' = 0.8939 e^{-180.8/RT} f_{H_2}^{0.0609} f_{CO_2}^{0.1248}\left(1 - \frac{f_{CH_3OH} f_{H_2O}}{f_{CO_2} f_{H_2}^3 K_{p_3^0}}\right)$ (55)
n_{H_2}	0.0609	
n_{CO_2}	0.1248	

The kinetic model found looks similar to the models discussed chapter 2. The Arrhenius constant for methanol formation reactions (1) and (3) are larger than the one for the RWGS, which was expected as the RWGS is a slow reaction. The two values however only slightly differ from one another, implying that carbon monoxide and carbon dioxide both act as carbon source for methanol. The equilibrium terms that are included in the model were evaluated for the outlet gas stream; in all three reactions the value was close to 0 indicating that the reactions are not close to their equilibrium, which justifies omitting the fugacity's of the reaction products. The RWGS could be described using only f_{H_2}. It was difficult to determine the parameters for this reaction. In the estimation all components orders received small values, of which hydrogen was the least small. The equilibrium term treats the hydrogen and carbon dioxide almost identically, but as the reaction is far from its equilibrium using only hydrogen was considered to be sufficient from the fitting results.

This power law model gives a more accurate prediction of the reaction rates for methanol. The parity plot of the best fitting estimation is shown below. The plot immediately shows better results for the power law than the LHHW model for methanol. The fit for water however is poor.

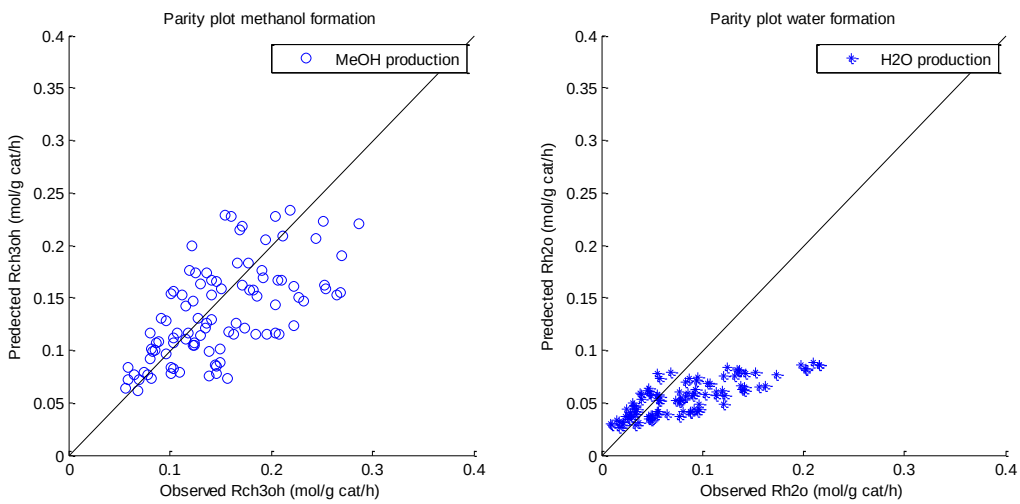

Figure 5-9 Parity plot of the power law model showing the predicted against the observed production rates of the kinetic experiments for methanol and water formation.

5.3.3 Power law model 2

The power law model proves to be a better model to describe the experimental data. Some of the recent kinetic models introduced in chapter 2 are based solely on reaction (2) and (3), claiming methanol is mainly formed through hydrogenation of carbon dioxide and carbon monoxide is primarily converted via the water gas shift. A third kinetic was therefore designed based on reaction (2) and (3) to compare to the previous model. The estimation was done in a similar way as the previous power law model, introducing the isotherm later on in the estimation. The results are displayed in Table 6, giving a $\Delta R'_{CH_3OH}$= 18.4 % for methanol and $\Delta R'_{H_2O}$ = 99.8 % for water. The parity plot is shown below in

Figure 5-10. The estimation for methanol seems to be even better than the previous model. For water however, the results are not as good for the same apparent reasons as in the previous estimation.

Table 6 Values for the fitted parameters of the power law based kinetic model containing reaction (2) and (3)

Parameter	Value	Kinetic model
A_{r2}	0.1077	
A_{r3}	1.4893	$r_2' = 0.1077e^{-133.2/RT} f_{H_2}^{0.0225}\left(1 - \frac{K_{p_2^0} f_{H_2O} f_{CO}}{f_{CO_2} f_{H_2}}\right)$ (56)
$E_{a,r2}$	-133.2	
$E_{a,r3}$	-180.8	
m_{H_2}	0.0225	$r_3' = 1.4893e^{-180.8/RT} f_{H_2}^{0.0751} f_{CO_2}^{0.1832}\left(1 - \frac{f_{CH_3OH} f_{H_2O}}{f_{CO_2} f_{H_2}^3 K_{p_3^0}}\right)$ (57)
n_{H_2}	0.0751	
n_{CO_2}	0.1832	

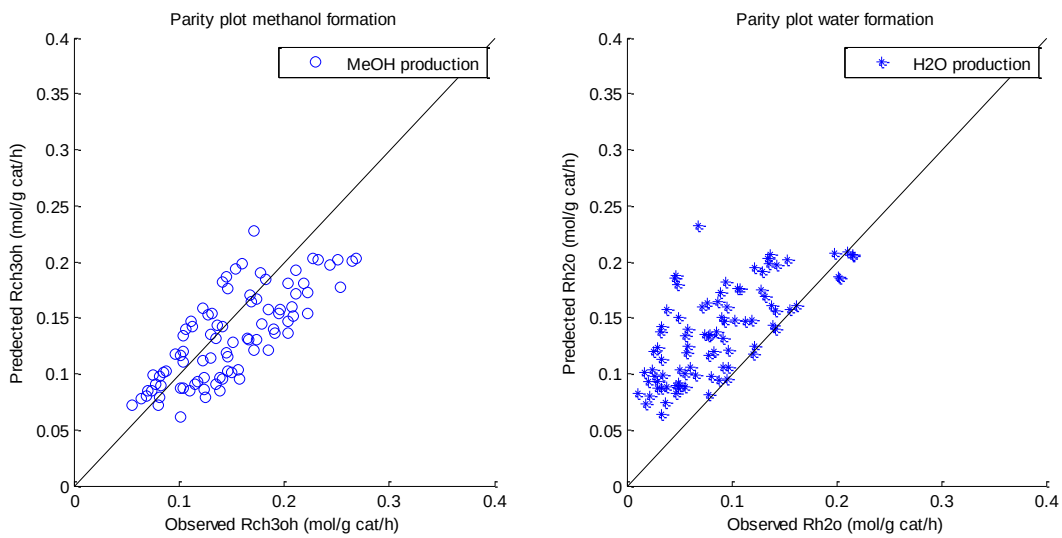

Figure 5-10 Parity plot of the power law model showing the predicted against the observed production rates of the kinetic experiments for methanol and water formation.

5.4 Comparison of derived models and discussion

The predicted production rates for methanol according to the three derived models are shown in Figure 5-11, the curves are the calculated values and the dots are the actual measured production rate. The LHHW-model shows no difference in prediction with different temperature as there is no temperature reference in the model. Both power laws do and give an adjusted prediction according to the experimental temperature. In this figure it can be clearly seen that the experiment done on 483 K are better described by power law model 2 than by the first power law model. The experiments done at 498 K are more difficult to be described as the production rate increases faster.

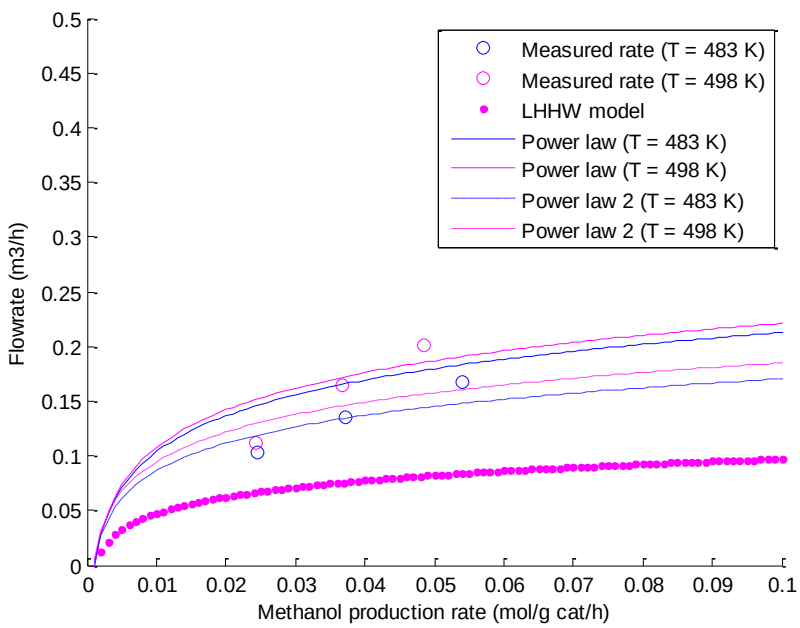

Figure 5-11 Methanol production rates according to all three derived models for syngas feed 4 ($H_2/CO/CO_2$ = 80.2/10.5/9.3 vol%, Sn = 3.6) for two experimental temperatures

The average error found for the kinetic models can be attributed to the experimental error and the choice of model. The reaction conditions for these experiments differ a lot from the conditions on which previous models are based. Even so, the first choice in selecting a kinetic model was the LHHW model. Unfortunately, it was not found possible to fit this simplified LHHW model to the data of the experiments. This was expressed in the high relative error found and difficulty in justifying the parameters obtained. A complex reason could be sought in the catalysts morphology to explain the orders of the adsorption term, but it is fair to say that the version of the LHHW model chosen here was not suitable for this dataset. Besides this, the dataset is limited

Both estimations using a power law based model show better results for methanol formation. The data points are closely placed around the diagonal of both parity plots and the relative average error gives a better value. The estimated orders for the fugacity's are very small, implying that variations in the reaction pressure have a small influence on the reaction rate. When the reaction rate and the reaction pressure were discussed in a previous paragraph, this phenomenon was

already seen in the plot. What is also interesting is that the data found for methanol formation is better described by the second power law model using only CO_2. This could be because the amount of CO_2 in the feed composition gives a better indication of the reaction rate than when both possible carbon sources are included into the equation. On the other hand, using only one carbon sources gives a less complicated model which could improve the fit. Nevertheless, the second power law gives an acceptable estimation of the production rates of methanol.

The prediction for water however is less accurate. When estimating the best fitting parameters, the SSR method was used in finding the best fitting parameter for methanol synthesis, which has an influence on the predicted value for water formation. The relative average error for the formation of water is in both models higher than the value for methanol. Water formation originates from reaction (2) and (3), of which the WGS reaction is ought to be slower than the methanol formation reaction. The distribution of the data in the parity plot is better for the second power law, even though the relative average error is larger. Looking at the parity plots for water formation, the dots do not surround the diagonal as expected for a good model. Large errors in the water concentration are common in modeling kinetics of methanol synthesis. The research done by Graaf et al included a comparison of kinetic models from other authors to his own and found that all models have a large error in the prediction of water formation [35]. His results are, together with this study listed in Table 7. This research has a rather good value for the prediction of water formation considering the other models.

Table 7 Errors for methanol and water production rates for various kinetic models. The experimental data, except for the data from this study were modeled with the model from Graaf [35]

Kinetic model from	$\Delta R'_{CH_3OH}$ (%)	$\Delta R'_{H_2O}$ (%)
Seyfert and Luft	10.8	100
Villa et al. [32]	12.3	100
Klier et al. [19]	10.0	57
Dybkjaer	14.7	167
Graaf et al. [35]	6.4	24
This study		
LHHW model	69.7	101.5
Power law model (T = 483 K)	19.2	47.3
Power law model (T = 498 K)	16.6	77.6
Power law model	23.7	42.3
Power law model 2	18.4	99.8

For methanol synthesis, the accuracy of the second power law model tends to previously published models. This model includes the reaction temperature, pressure and gas composition and flow rate. An important note to be made is that this model is based on only two experimental temperatures. This model is valid for temperatures of 483 K to 498 K and extrapolation has not been examined.

Experimental errors may have many origins. The methanol formation reactions in the Supermethanol region are very fast. Upon leaving the reactor, the effluent stream expands from 17.5 – 22.5 MPa to atmospheric pressure, the occurring

Joule-Thompson effect cools down the effluent gas. Depending on the local concentration of methanol and water, the effluent gas can be very close to its vapor-liquid equilibrium causing condensation in system. The line from the reactor to the GC was traced with 130 °C to prevent condensation. Nevertheless, droplets of methanol and water showed on the GC data as a sudden increased methanol and water value making these experiments invalid for this study. To prevent this from happening, the amount of catalyst was lowered so valid data could be collected. A smaller amount of catalyst lowered the chances of condensation; unfortunately also a smaller measuring window is created with relative larger measuring errors. In obtaining the experimental data, the deactivation of the catalyst was assumed to be negligible. This assumption was based on a long duration experiment without varying the temperature, pressure and flow in which the methanol concentration in the outlet remained constant. In some experiments however, the methanol concentration can be interpreted as decreasing or increasing slightly. This is the most pronounced for the experiments at the higher temperatures. If decreasing concentration is caused by deactivation it might be an additional explanation for the difficulties in obtaining a very accurate data fit. A more detailed investigation of this phenomenon should definitely be part of future research.

Adsorption of one of the products on the catalyst surface or condensation inside the catalyst is also not unthinkable and would have a large inhibiting effect on the methanol formation rate. Fluctuations in the syngas feed to the reactor can also have an influence on the results, but the effect was not measured and therefore neglected. The calibration of the GC used in the experiments was done with wash bottles containing the liquid reaction products. Saturation of the N_2 stream was verified by using different flow rates, but this method induces an error. Furthermore, a single point calibration was done at room temperature at which the methanol concentration is significantly higher than the average concentration measured during the kinetic experiments.

While conducting the experiments, the composition of the reactor effluent gas was determined on line. The methanol concentration in the effluent stream is expected to decreases when the feed gas flow increased. This was observed for most experiments, however for some of the experiments carried out at T = 513 K the opposite was observed and is shown in Figure 5-12. This is not expected and difficult to explain. The increased concentration could be caused by a higher than anticipated catalyst temperature, where the exothermic formation reactions increase the catalysts temperature and increasing the production rate. However this is unlikely, a local temperature gradient over the catalyst was ruled out by an experiment using a mixture of catalyst and inert grid. In addition, the small amount of catalyst, fast rotational speed and high flow rate of the reaction gas would make this improbable.

When looking at the water formation rate, a decrease in production is seen with increasing temperature. The decrease in water formation could be explained by CO as the methanol carbon source instead of CO_2. If this is the case, a turning point in the reaction mechanism lies somewhere around this temperature. In Chapter 2 the reaction equilibria were discussed noting that methanol formation is more favorable at low temperatures and the WGS equilibrium is less temperature dependent. The WGS reaction is however more favorable with increasing temperature. During the parameter estimation, the water formation in the experiments was largely ascribed to methanol formation from CO_2, as

the methanol formation reaction is much faster than the RWGS. Another explanation to the decrease of water in the effluent stream is that with increasing temperature, the faster WGS converts more water to CO_2. The additional CO_2 in the reactor than gives a higher methanol concentration in the outlet. The explanation of the increased methanol production rate with increasing flow however is not clear and as the origin of these phenomena cannot be explained in accordance with the model, nor with the kinetic dataset obtained during the experiments, the higher temperature experiments were not considered in the estimation of the parameters.

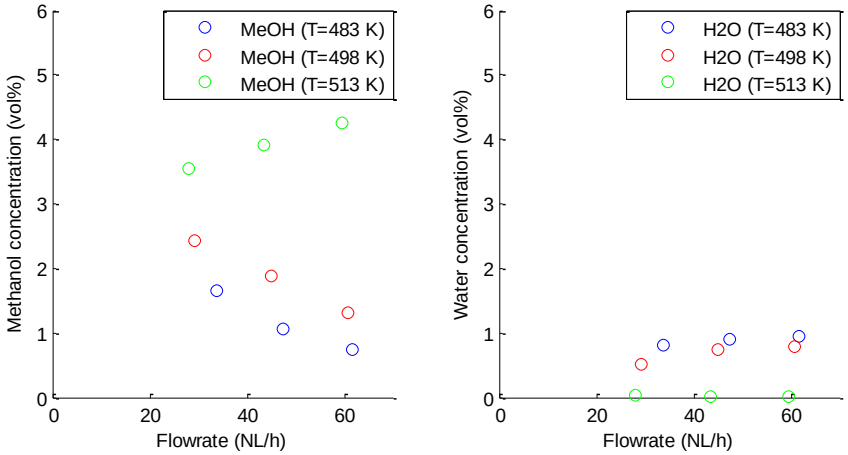

Figure 5-12 Methanol and water concentration as a function of the exit flow for syngas H2/CO/CO2 = 68.1/27.3/4.6.

More experiments are advised to gain better understanding of the reaction mechanism as the reaction pathway is not fully understood around the reaction conditions of the Supermethanol process. A more robust setup is recommended to ensure no condensation of methanol or water in the system. A larger gas buffer could be used in the setup to narrow down the fluctuations in the ingoing gas feed, as the influence of concentration fluctuations were in this case neglected. Deactivation was also neglected during the experiments. Fresh catalyst was used daily, but feed gases and experimental conditions were varied throughout the day, its effect on the catalyst is worth examining. The GC calibration was done thoroughly, however at room temperature, containing higher water and methanol concentrations than encountered during the experiments. The accuracy of the obtained data could therefore be questioned.

While fitting the LHHW model to the experimental data, the results did not benefit from the addition of term for water in the adsorption term. Water is known to have an inhibiting effect on the reaction rate and should therefore be present in the adsorption term. With the introduction of the power law in chapter 2, two inhibition terms were included in the equation for both methanol and water. As the dataset was too limited, both power law models do not include inhibition terms. Adding an inhibition term to a future model could help its reliability.

Summarizing, in this thesis high pressure methanol was investigated. This appeared to be more difficult than anticipated on forehand. It was difficult to explain the trends in the dataset and the behavior in general of methanol synthesis (in this set-up). Therefore, the dataset should be considered as a rough dataset due to all the issues/topics raised in this

discussion and the extreme conditions. Nevertheless this is one of the first research studies to high pressure methanol synthesis and although the errors and uncertainties might be higher than strived for initially, the data was used to derive the first kinetic models for high pressure methanol synthesis over a copper based catalyst. The power law models derived can be used as a preliminary model for kinetics of high pressure methanol synthesis, but needs to be improved and made more accurate in future studies.

6 Conclusion

The reaction rates for high pressure methanol synthesis form CO, CO_2 and H_2 were studied in a continuous spinning basket reactor. The datasets were obtained from experiments conducted at 17.5 to 22.5 MPa and 483-498 K. Two kinetics models were used in modeling the methanol synthesis resulting in a best fitting power law with a relative average error for methanol of 18.4%, which is in line with previously published models. Even though a power law model was required to obtain a suitable fit, this model is the first of its kind to for methanol synthesis under these conditions.

Most published kinetic models are developed for low pressure methanol synthesis. The kinetics obtained in this study are a good starting point in high pressure methanol synthesis as it is the first of its kind using a commercial $Cu/ZnO/Al_2O_3$ catalyst. Gathering reliable data under these circumstances however presented challenges as the reactions rates were fast and condensation occurred easily in the experimental setup. Experiments conducted at higher temperatures showed that the reaction mechanism is much more complex than known so far. As the complexity cannot be translated to the kinetic model, a power law had to be used. More understanding of the reaction system and phenomena (in particular the absence or presence of deactivation) and accuracy of the measurements is required to measure and derive a more detailed kinetic description.

7 Notation

a	Attractive parameter of EOS
A_i	Arrherius factor
$A = \frac{aP}{R^2T^2}$	Reduced attractive parameter of EOS
b	Repulsive parameter of EOS
$B = \frac{bP}{RT}$	Reduced repulsive parameter of EOS
D	Diffusion coefficient *(m^2/s)*
E_a	Activation energy *(J/mol)*
f	Fugacity
ΔG_r	Gibbs free energy
ΔH_r	Reaction enthalpy
k	Reaction rate constant
K_P	Chemical equilibrium constant based on pressure
K_ϕ	Deviation of K_P from the ideal gas law
K_f	Chemical equilibrium constant based on fugacity *(Pa)*
m	Characteristic constant
N	Number of measurements
p	Polar parameter
P	Pressure *(Pa)*
r	Radius *(m)*
r	Reaction
r'	Reaction rate per weight of catalyst *(mol/gr. cat/h or gram/gr. cat/h)*
R	Universal gas constant *(8.314 J/mol/K)*
R'	Production rate *(mol/gr. cat/h or gram/gr. cat/h)*
S_N	Syngas stoichiometric ratio
SSR	Sum of squared residuals
T	Absolute temperature *(K)*
y_i	Mole fraction
V	Volume *(m^3)*
w	Catalyst weight *(kg)*
WF	Weighing factor
Z	Compressibility
a	A-dimensional factor for a
Δ	Relative error
H	Effectiveness factor
ξ	Inhibition term *(Pa)*
σ	Standard deviation
Σ	Sum
ϕ_v	Volumetric flow
φ_i	Fugacity coefficient
ω_i	Acentric factor

Superscripts

^	Indicates calculated value
0	Indicates standard pressure
l,m,n	Fit parameter
V	Indicates vapor phase

Subscripts

c	Critical property
$cat.$	Catalyst
i,j	Indicates component
in	Indicates flow in
$liq.$	Liquid
Off	Indicates exit flow
P	Indicates partial pressure
v	Indicates volumetric

8 References

[1] Het Europees Parlement en de raad van de Europeese Unie, "Richtlijn 2009/28/EG van het Europees Parlement van de Europeese Unie ter bevordering van het gebruik van energie uit hernieuwbare bronnen en houdende wijziging en intrekking van Richtlijn 2001/77/EG en Richtlijn 2003/30/EG," 23 april 2009. [Online]. Available: http://eur-lex.europa.eu/LexUriServ/LexUriServ.do?uri=OJ:L:2009:140:0016:0062:NL:PDF. [Accessed 15 december 2012].

[2] A. Singhabhandhu and T. Tezuka, "A perspective on incorporation of glycerin purification process in biodiesel plants using waste cooking oil as feedstock," *Energy,* vol. 35, no. 6, p. 2493–2504, 2010.

[3] zeep.com, "ZEEP - The methanol opportunity," zeep.com, 2013. [Online]. Available: http://www.zeep.com/market-opportunity.html. [Accessed 15 July 2013].

[4] J. van Bennekom, R. Venderbosch, D. Assink and H. Heeres, "Reforming of methanol and glycerol in supercritical water," *Journal of Supercritical Fluids,* no. 58, pp. 99-113, 2011.

[5] J. van Bennekom, V. Kirillov, Y. Amosov, T. Krieger, R. Venderbosch, D. Assink, K. Lemmens and H. Heeres, "Explorative catalyst screening studies on reforming of glycerol in supercritical water," *Journal of Supercritical Fluids,* no. 70, pp. 171-181, 2012.

[6] J. B. Hansen and P. E. Nielsen, "Methanol Synthesis," in *Handbook of heterogeneous catalysis*, Weinheim, Germany, Wiley-VCH Verlag GmbH & Co., 2008, pp. 2920-2943.

[7] S. Lee, Methanol synthesis technology, Boca Raton, Florida: CRC Press Inc., 1990.

[8] J. Moulijn, M. Makkee and A. van Diepen, Chemical Process Technology, West Sussex, England: John Wiley & Sons Ltd, 2001.

[9] M. Institute, "Methanol Basics, the methanol industry," Methanol Institute, 2011. [Online]. Available: http://www.methanol.org/Methanol-Basics/The-Methanol-Industry.aspx. [Accessed 16 Augustus 2012].

[10] J. van Bennekom, R. Venderbosch, D. Assink, K. Lemmens and H. Heeres, "Bench scale demonstration of the Supermethanol concept: The synthesis of methanol from glycerol derived syngas," *Chemical Engineering Journal,* no. 207-208, pp. 245-253, 2012.

[11] P. Atkins and J. De Paula, "Chemical equilibria," in *Aktinks´ Physical Chemistry*, Oxford, Oxford University Press, 2006, pp. 845-858.

[12] J. van Bennekom, R. Venderbosch, D. Assink, K. Lemmens, J. Winkelman, E. Wilbers and H. Heeres, "Methanol synthesis beyond chemical equilibrium," *Chemical Engineering Sci. ,* no. 87, pp. 204-208, 2013.

[13] J. Hansen and P. Nielsen, "Methanol Synthesis," in *Handbook of Heterogeneous Catalysts*, Weinheim, Germany , Wiley and Sons, Ltd, 2008, pp. 2920-2949.

[14] L. Lloyd, "Methanol Synthesis," in *Handbook of Industrial Catalysts*, New York, Springer Science Business Media, LLC,

2011, pp. 421-437.

[15] H. Scott Fogler, "External diffusion effects on heterogeneous catalysis," in *Elements of chemical reaction engineerging*, Westford, Massachussets, Pearson education Ltd., 2006, pp. 757-811.

[16] C. Brown and C. Bennet, "Methanol synthesis catalysis in an internally recycled reactor," *AIChE Journal,* pp. Vol. 16, No, 5, p 817-823, 1970.

[17] G. Chinchen, K. Waugh and D. Whan, "The activity of and state of the copper surface in methanol synthesis catalysis," *Applied Catalysis,* no. 25, pp. 101-107, 1986.

[18] H. Wilmer and O. Hinrichsen, "Dynamical changes in Cu/ZnO/Al2O3 catalysts," *Catalysis Letters,* no. 82, pp. 117-122, 2002.

[19] K. Klier, V. Chatikavanij, R. Herman and G. Simmons, "Catalytic synthesis of methanol from CO/H2," *Journal of Catalysis,* no. 74, pp. 343-360, 1982.

[20] K. Topsoe, C. Ovesen, B. Clausen, N. Topsoe, P. Nielsen, E. Tornqvist and J. Norskov, "Importance of dynamics in real catalyst systems," in *Dynamics of Surfaces and Reaction Kinetics in Heterogeneous Catalysis, Studies in Surface Science and Catalysis*, Amsterdam, The Netherlands, Elsevier , 1997, pp. 121-139.

[21] C. Peter, B. Vesborga, I. Chorkendorffa, I. Knudsena, O. Balmesb, J. Nerlovb, A. Molenbroek, B. Clausenb and S. Helvegb, "Transient behavior of Cu/ZnO-based methanol synthesis catalysts," *Journal of Catalysis,* no. 262, pp. 65-72, 2009.

[22] N. Topsoe and H. Topsoe, "On the nature of surface structural canges in Cu/ZnO methanol synthesis catalysts," *Topics in Catalysis,* no. 8, pp. 267-270, 1999.

[23] T. Fujitani and J. Nakamura, "The effect of ZnO in methanol catalysis on Cu dispersion and specific activity," *Catalysis Letters,* no. 56, pp. 119-124, 1998.

[24] Y. Choi, J. Nakamura, T. Fujitani and K. Futagami, "The role of ZnO in Cu/ZnO methanol synthesis catalysts - morphology effect or active site model?," *Applied catalysis,* no. 208, pp. 163-167, 2001.

[25] J. Nakamura, Y. Choi and T. Fuijitani, "On the issue of the active site and the role of ZnO in Cu/ZnO methanol synthsis catalysis," *Topics in Catalysis,* no. 22, pp. 277 - 285, 2003.

[26] G. Graaf, P. Sijtsema, E. Stamhuis and G. Joosten, "Chemical equilibria in methanol synthesis," *Chemical Engineering Science,* pp. Vol. 41, No. 11, pp. 2883-2890, 1986.

[27] S. Lee, "Methanol synthesis from syngas," in *Handbook of alternative fuel technology*, Boca Raton, Taylor & Francis Group, LLC, 2007, pp. 297-321.

[28] T. Askgaard, J. Norskov, C. Ovesen and P. Stoltze, "A kinetic model of methanol synthesis," *Journal of Catalysis,* pp. No. 156, pp. 229-242, 1995.

[29] P. Stoltze and J. Norskov, "Theoretical modeling of catalytic reactions," in *Handbook of heterogeneous catalysis*,

Weinheim, Germany, Wiley, 2008, pp. 1479-1489.

[30] J. Skrzypek, J. Sloczynski and S. Ledakowicz, Methanol Synthesis, Warszawa, Poland: Polish Scientific Publishers, 1994.

[31] H. Bakemeier, P. Laurer and W. Schroder, "Development and application of a mathematical model of the methanol synthesis," *Chemical Engineering Progress Symposium Series,* pp. Vol. 66, No. 98, pp. 1-10, 1970.

[32] P. Villa, P. Forzatti, G. Buzzi-Ferraris, G. Garone and I. Pasquon, "Synthesis of alcohols from carbon oxides and hydogen. 1. Kinetics of low pressure methanol synthesis," *Ind. Eng. Chem. Process Des. Dev. ,* no. 24, pp. 12-19, 1985.

[33] K. Vanden Bussche and G. Froment, "A steady-state kinetic model for methanol syntheiss and the water gas shift reaction on a commercial Cn/ZnO/Al2O3 catalyst," *Journal of catalysis,* no. 161, pp. 1-10, 1996.

[34] J. Skrzypek, M. Lachowska and M. H., "Kinetics of methanol synthesis over commercial copper/zinc oxide/alumina catalyst," *Chemical Engineering Science,* pp. Vol. 46, No. 11, pp. 2890-2813, 1991.

[35] G. Graaf, E. Stamhuis and A. Beenackers, "Kinetics of low-pressure methanol synthesis," *Chemical Engineering Science,* pp. Vol. 43, No. 12, pp 3185-3195, 1988.

[36] D. Newsom, "The water-gas-shift reaction," *Chemical Reviews Science and Engineering,* pp. Vol. 21, No. 2, pp. 275-318, 1980.

[37] F. Helfferich, "Chapter 9 Heterogeneous Catalysis," in *Kinetics of multistep reactions*, Pennsylvania State University, Elsevier, 2004, pp. 273-295.

[38] G. Graaf, H. Scholtens, E. Stamhuis and A. Beenackers, "Intra-particle diffusion limitations in low-pressure methanol synthesis," *Chemical Engineering Science,* pp. Vol. 45, No. 4, p 773-783, 1990.

[39] I. Melian Cabrera, "Course: Design of industrial catalysts," in *Fundamentals, Design of industrial catalysts*, RuG, Groningen, the Netherlands, 2012.

[40] M. Behrens, F. Studt, I. Kasatkin, S. Kuhl, M. Havecker, F. Abild-Pedersen, S. Zander, F. Girgsdies, P. Kurr, B. Kniep, Tovar, R. Fischer, J. Norskov and R. SChlogl, "The active site of methanol synthesis over Cu/ZnO/Al2O3 industrial catalysts," *Science,* no. 336, pp. 893-897, 2012.

9 Appendices

9.1 Adsorption equilibia, elementary reactions and driving forces

Table 8 Adsorption equilibria, elementary reactions and driving forces of methanol synthesis reaction (1), (2) and (3) according to [35].

Adsorption equilibria	
$CO + s1 = CO\,s1$	
$CO_2 + s1 = CO_2\,s1$	
$H_2 + 2\,s2 = 2\,Hs2$	
$H_2O + s2 = H_2O + s2$	
Elementary reactions	**Driving force**
Reaction (1)	
1.1: $COs1 + Hs2 = HCOs1 + s2$	$f_{CO}f_{H_2}^{1/2} - f_{CH_3OH}/(f_{H_2}^{3/2}K_{p_1}^0)$
1.2: $HCOs1 + Hs2 = H_2COs1 + s2$	$f_{CO}f_{H_2} - f_{CH_3OH}/(f_{H_2}K_{p_1}^0)$
1.3: $H_2COs1 + Hs2 = H_3COs1 + s2$	$f_{CO}f_{H_2}^{3/2} - f_{CH_3OH}/(f_{H_2}^{1/2}K_{p_1}^0)$
1.4: $H_3COs1 + Hs2 = CH_3OH + s1 + s2$	$f_{CO}f_{H_2}^{1/2} - f_{CH_3OH}/K_{p_1}^0$
Reaction (2)	
2.1: $CO_2s1 + Hs2 = HCO_2s1 + s2$	$f_{CO_2}f_{H_2}^{1/2} - f_{CO}f_{H_2O}/(f_{H_2}^{1/2}K_{p_2}^0)$
2.2: $HCO_2s1 + Hs2 = COs1 + H_2Os2$	$f_{CO_2}f_{H_2} - f_{CO}f_{H_2O}/K_{p_2}^0$
Reaction (3)	
3.1: $CO_2s1 + Hs2 = HCO_2s1 + s2$	$f_{CO_2}f_{H_2}^{1/2} - f_{CH_3OH}f_{H_2O}/(f_{H_2}^{5/2}K_{p_3}^0)$
3.2: $HCO_2s1 + Hs2 = H_2CO_2s1 + s2$	$f_{CO_2}f_{H_2} - f_{CH_3OH}f_{H_2O}/(f_{H_2}^{2}K_{p_3}^0)$
3.3: $H_2CO_2s1 + Hs2 = H_3CO_2s1 + s2$	$f_{CO_2}f_{H_2}^{3/2} - f_{CH_3OH}f_{H_2O}/(f_{H_2}^{3/2}K_{p_3}^0)$
3.4: $H_3CO_2s1 + Hs2 = H_2COs1 + H_2Os2$	$f_{CO_2}f_{H_2}^{2} - f_{CH_3OH}f_{H_2O}/(f_{H_2}K_{p_3}^0)$
3.5: $H_2CO + Hs2 = H_3COs1 + s2$	$f_{CO_2}f_{H_2}^{5/2}/f_{H_2O} - f_{CH_3OH}/(f_{H_2}^{1/2}K_{p_3}^0)$
3.6: $H_3COs1 + Hs2 = CH_3OH + s1 + s2$	$f_{CO_2}f_{H_2}^{2}/f_{H_2O} - f_{CH_3OH}/K_{p_3}^0$

9.2 Kinetic data used in the derivation of the kinetic model

Feed-run	Conditions		Exit									
	P	T	H_2	CO	CO_2	CH_3OH	H_2O	CH_4	cat used	$\phi_{V,off}$	R'_{CH_3OH}	R'_{H_2O}
	MPA	K	vol%	vol%	vol%	vol%	vol%	vol%	g	NL/h	g/g cat/h	g/g cat/h
1-1	17.19	483.55	66.48	26.48	4.24	1.58	0.72	0	0.2016	25.58	2.59	0.66
1-2	17.09	483.45	66.96	27.10	3.75	1.16	0.80	0	0.2016	37.87	2.82	1.09
1-3	17.45	483.45	67.58	27.45	3.32	0.85	0.65	0	0.2016	50.27	2.74	1.18
1-4	19.89	483.75	67.53	28.22	2.15	1.10	0.52	0	0.1969	31.32	2.27	0.60
1-5	19.90	483.55	64.70	31.18	2.57	0.83	0.47	0	0.1969	43.82	2.40	0.76
1-6	19.97	483.65	67.12	29.04	2.50	0.71	0.47	0	0.1969	57.83	2.69	1.01
1-7	22.58	483.65	67.26	27.72	2.80	1.20	0.61	0	0.2005	30.77	2.38	0.68
1-8	22.63	483.65	67.43	27.69	3.18	0.92	0.58	0	0.2005	45.97	2.73	0.96
1-9	22.59	483.65	67.71	27.75	3.11	0.76	0.53	0	0.2005	61.85	3.05	1.18
1-10	17.81	498.55	66.51	26.15	3.85	3.09	0.19	0	0.2016	24.23	4.80	0.17
1-11	17.75	498.45	66.35	25.98	3.96	3.54	0.05	0	0.2016	36.88	8.38	0.07
1-12	17.82	498.55	66.29	26.23	3.57	3.77	0.05	0	0.2016	50.83	12.28	0.09
1-13	19.94	498.65	67.00	27.81	2.49	2.02	0.49	0	0.1969	34.15	4.53	0.61
1-14	20.00	498.65	67.48	27.72	2.56	1.48	0.64	0	0.1969	42.95	4.19	1.02
1-15	20.02	498.65	68.00	27.83	2.38	1.11	0.61	0	0.1969	57.84	4.20	1.30
1-16	22.69	498.65	66.73	27.26	3.19	2.20	0.47	0	0.2005	30.35	4.32	0.52
1-17	22.71	498.75	66.83	27.46	3.20	1.81	0.61	0	0.2005	45.85	5.35	1.01
1-18	22.75	498.75	67.25	27.57	2.99	1.40	0.72	0	0.2005	61.63	5.57	1.61
2-1	17.80	483.55	61.80	22.58	13.28	1.57	0.53	0	0.2057	20.96	2.06	0.39
2-2	17.86	483.55	61.48	23.18	13.35	1.29	0.56	0	0.2057	31.57	2.57	0.63
2-3	17.67	483.55	61.88	23.30	13.08	1.04	0.62	0	0.2057	42.31	2.77	0.93
2-4	20.22	483.65	61.68	22.32	13.59	1.61	0.46	0	0.2005	26.23	2.73	0.44
2-5	20.01	483.65	61.96	21.98	13.88	1.39	0.61	0	0.2005	40.00	3.57	0.89
2-6	20.08	483.65	61.68	23.18	13.24	1.09	0.71	0	0.2005	58.52	4.10	1.51
2-7	22.77	483.65	62.42	22.99	12.99	0.94	0.26	0	0.1007	27.74	3.33	0.53
2-8	22.72	483.65	62.23	22.98	13.35	0.89	0.29	0	0.1007	41.27	4.70	0.88
2-9	22.78	483.65	62.36	23.06	13.29	0.79	0.32	0	0.1007	54.26	5.50	1.24
2-10	17.82	498.55	61.54	23.47	12.71	1.45	0.48	0	0.1057	27.05	4.80	0.90
2-11	17.76	498.55	68.80	16.77	12.34	1.32	0.59	0	0.1057	40.46	6.54	1.64
2-12	17.71	498.55	64.95	20.42	12.67	1.13	0.71	0	0.1057	56.56	7.81	2.75
2-13	20.33	498.55	62.77	22.35	12.91	1.20	0.64	0	0.1057	26.95	3.96	1.18
2-14	20.34	498.55	62.33	22.54	12.99	1.16	0.66	0	0.1057	40.53	5.73	1.85
2-15	20.24	498.55	62.04	22.55	13.33	1.02	0.69	0	0.1057	54.03	6.77	2.57
2-16	22.72	498.65	62.01	23.12	13.32	0.98	0.31	0	0.1007	26.33	3.33	0.59
2-17	22.82	498.65	61.74	23.01	13.30	1.26	0.47	0	0.1007	41.11	6.63	1.39
2-18	22.78	498.65	61.96	22.99	13.12	1.14	0.62	0	0.1007	55.19	8.05	2.46
3-1	17.62	483.65	71.98	16.93	8.42	1.41	0.85	0	0.1968	28.57	2.65	0.89
3-2	17.64	483.55	72.16	18.52	6.94	1.12	0.93	0	0.1968	44.89	3.32	1.55
3-3	17.66	483.65	72.69	19.21	6.05	0.90	1.00	0	0.1968	61.21	3.61	2.26
3-4	19.92	483.95	72.83	19.47	5.61	1.02	0.77	0	0.1081	30.43	3.70	1.58
3-5	19.95	483.85	72.91	19.44	5.92	0.83	0.66	0	0.1081	45.65	4.51	2.04
3-6	19.95	483.95	73.30	19.56	5.73	0.69	0.58	0	0.1081	62.05	5.14	2.43
3-7	22.48	483.85	72.56	19.56	5.85	0.98	0.79	0	0.1025	30.65	3.78	1.72
3-8	22.52	483.75	72.96	19.48	5.95	0.76	0.67	0	0.1025	45.47	4.38	2.15
3-9	22.49	483.75	73.35	19.54	5.76	0.66	0.57	0	0.1025	59.86	4.95	2.44
3-10	17.69	498.65	71.54	18.88	6.17	2.05	0.92	0	0.1968	29.62	3.99	1.01
3-11	17.67	498.65	71.94	19.15	6.02	1.64	1.00	0	0.1968	44.89	4.83	1.65
3-12	17.66	498.65	72.28	19.36	5.82	1.35	1.03	0	0.1968	60.41	5.37	2.31
3-13	20.01	498.95	72.46	19.41	5.73	1.40	0.76	0	0.1081	31.16	5.20	1.59
3-14	19.79	498.95	72.81	19.58	5.59	1.11	0.82	0	0.1081	46.09	6.14	2.55
3-15	19.34	499.45	71.10	21.12	5.93	0.89	0.88	0	0.1081	61.37	6.53	3.65
3-16	22.82	498.85	72.59	19.51	5.76	1.32	0.68	0	0.1025	30.40	5.07	1.46
3-17	22.73	498.75	72.60	19.55	5.92	1.06	0.77	0	0.1025	45.66	6.10	2.51
3-18	22.70	498.75	72.82	19.49	5.82	0.92	0.85	0	0.1025	60.46	7.02	3.64
4-1	17.56	483.45	78.75	10.32	8.96	1.41	0.45	0	0.2005	19.72	1.79	0.32
4-2	17.67	483.55	78.76	10.45	9.03	1.22	0.49	0	0.2005	39.59	3.10	0.71
4-3	17.64	483.45	78.83	10.48	8.95	1.16	0.54	0	0.2005	53.92	4.03	1.05
4-4	20.32	483.45	78.35	10.50	9.35	1.10	0.54	0	0.1054	24.51	3.31	0.90
4-5	20.46	483.45	78.48	10.48	9.45	0.96	0.56	0	0.1054	37.12	4.35	1.42
4-6	20.54	483.55	78.67	10.45	9.37	0.86	0.59	0	0.1054	54.00	5.71	2.19
4-7	22.70	483.65	78.99	10.26	9.36	0.83	0.19	0	0.1008	22.44	2.40	0.31
4-8	22.74	483.55	78.74	10.47	9.56	0.81	0.25	0	0.1008	33.03	3.43	0.59
4-9	22.75	483.55	78.88	10.46	9.48	0.81	0.26	0	0.1008	43.50	4.52	0.81
4-10	17.50	498.45	78.70	10.57	8.95	1.19	0.53	0	0.1054	24.19	3.53	0.88
4-11	17.52	498.45	78.76	10.55	8.89	1.22	0.54	0	0.1054	37.40	5.59	1.40
4-12	17.53	498.45	78.64	10.48	9.11	1.17	0.57	0	0.1054	49.57	7.11	1.95
4-13	20.59	498.55	78.71	10.62	9.06	1.09	0.50	0	0.1054	24.29	3.24	0.84
4-14	20.39	498.55	78.43	10.53	9.31	1.17	0.53	0	0.1054	36.75	5.29	1.33
4-15	20.44	498.55	78.37	10.48	9.43	1.13	0.57	0	0.1054	48.54	6.75	1.89
4-16	22.64	498.45	78.88	10.65	9.19	0.91	0.24	0	0.1008	21.58	2.51	0.37
4-17	22.80	498.55	78.59	10.61	9.47	1.02	0.25	0	0.1008	31.94	4.17	0.57
4-18	22.77	498.55	78.52	10.53	9.60	1.03	0.27	0	0.1008	44.12	5.83	0.85

Feed-run	Conditions		Exit									
	P	T	H_2	CO	CO_2	CH_3OH	H_2O	CH_4	cat used	$\phi_{V,off}$	R'_{CH_3OH}	R'_{H_2O}
	MPA	K	vol%	vol%	vol%	vol%	vol%	vol%	g	NL/h	g/g cat/h	g/g cat/h
5-1	17.53	483.35	87.44	5.19	5.25	1.18	0.31	0	0.2053	25.52	1.90	0.28
5-2	17.48	483.35	87.64	5.20	5.20	1.17	0.40	0	0.2053	38.58	2.84	0.55
5-3	17.46	483.35	88.41	5.23	4.80	0.93	0.46	0	0.2053	51.95	3.04	0.85
5-4	20.15	483.75	88.10	5.23	4.77	1.02	0.47	0	0.2007	28.50	1.87	0.48
5-5	20.34	483.65	87.91	5.21	5.10	1.03	0.45	0	0.2007	44.11	2.93	0.72
5-6	20.45	483.65	88.12	5.21	4.98	1.00	0.47	0	0.2007	59.42	3.81	1.01
5-7	22.55	483.75	88.47	5.23	4.74	0.92	0.47	0	0.2007	28.98	1.71	0.49
5-8	22.64	483.75	88.64	5.27	4.58	0.96	0.45	0	0.2007	42.62	2.65	0.70
5-9	22.80	483.75	88.49	5.22	4.68	0.95	0.45	0	0.2007	57.73	3.54	0.93
5-10	17.60	498.65	88.04	4.69	4.78	1.57	0.25	0	0.2007	21.80	2.20	0.19
5-11	17.63	498.65	87.90	4.99	4.96	1.40	0.37	0	0.2007	34.21	3.10	0.46
5-12	17.59	498.65	87.90	5.14	4.82	1.38	0.41	0	0.2007	45.97	4.08	0.69
5-13	20.13	498.55	87.96	4.55	5.26	1.35	0.26	0	0.1007	25.72	4.46	0.49
5-14	20.13	498.75	88.01	5.04	5.01	1.29	0.37	0	0.1007	39.45	6.53	1.05
5-15	20.12	498.85	88.20	5.17	4.79	1.18	0.44	0	0.1007	53.48	8.13	1.70
5-16	22.55	483.75	88.47	5.23	4.74	0.92	0.47	0	0.2007	28.98	1.71	0.49
5-17	22.64	483.75	88.64	5.27	4.58	0.96	0.45	0	0.2007	42.62	2.65	0.70
5-18	22.80	483.75	88.49	5.22	4.68	0.95	0.45	0	0.2007	57.73	3.54	0.93
6-1	17.81	483.55	83.42	12.15	1.67	1.98	0.66	0	0.1963	24.89	3.25	0.60
6-2	17.76	483.55	83.24	12.77	1.83	1.28	0.82	0	0.1963	46.56	3.94	1.41
6-3	17.81	483.55	83.58	12.88	1.88	0.95	0.68	0	0.1963	62.86	3.92	1.57
6-4	20.01	483.75	83.07	12.44	2.35	1.30	0.74	0	0.1945	30.52	2.63	0.84
6-5	19.88	483.65	83.10	12.76	2.18	1.04	0.86	0	0.1945	46.70	3.24	1.49
6-6	20.00	483.65	83.41	12.94	2.01	0.81	0.79	0	0.1945	62.75	3.38	1.86
6-7	22.15	483.65	83.25	13.27	1.69	1.08	0.68	0	0.1094	31.16	3.99	1.40
6-8	21.95	483.65	83.26	13.22	1.83	0.97	0.70	0	0.1094	47.54	5.48	2.20
6-9	21.93	483.65	83.68	13.29	1.71	0.73	0.57	0	0.1094	62.77	5.42	2.38
6-10	17.07	498.35	83.58	10.99	1.86	3.36	0.15	0	0.1963	29.82	6.61	0.17
6-11	16.96	498.55	82.80	11.73	1.82	3.44	0.19	0	0.1963	45.27	10.25	0.31
6-12	17.06	498.65	83.09	12.52	1.57	2.13	0.66	0	0.1963	61.38	8.63	1.50
6-13	19.77	498.55	83.22	11.92	2.13	2.20	0.48	0	0.1945	30.29	4.44	0.54
6-14	19.60	498.65	82.91	12.54	1.97	1.94	0.60	0	0.1945	46.15	5.95	1.04
6-15	19.43	498.65	83.19	12.80	1.75	1.50	0.73	0	0.1945	62.65	6.24	1.72
6-16	22.10	498.65	83.15	12.81	1.68	1.79	0.55	0	0.1094	30.48	6.43	1.12
6-17	22.38	498.65	83.03	13.02	1.80	1.47	0.66	0	0.1094	46.65	8.08	2.06
6-18	22.43	498.65	83.27	13.11	1.64	1.22	0.74	0	0.1094	63.79	9.17	3.13
7-1	17.31	483.55	84.81	1.32	11.67	1.15	0.94	0	0.2025	30.19	2.22	1.02
7-2	17.90	483.45	84.08	1.34	12.53	0.97	1.05	0	0.2025	44.44	2.76	1.67
7-3	17.87	483.45	84.66	1.26	12.04	0.97	1.05	0	0.2025	59.51	3.70	2.23
7-4	20.01	483.55	86.12	1.24	10.65	1.07	0.89	0	0.1023	34.51	4.69	2.18
7-5	19.98	483.55	85.00	1.24	11.80	1.07	0.88	0	0.1023	46.43	6.29	2.92
7-6	19.97	483.55	85.04	1.19	11.86	0.98	0.91	0	0.1023	59.81	7.44	3.89
7-7	22.29	483.55	84.60	1.27	12.12	1.15	0.76	0	0.1065	33.43	4.65	1.74
7-8	22.16	483.55	84.88	1.23	11.95	1.08	0.81	0	0.1065	45.17	5.92	2.49
7-9	22.21	483.55	84.88	1.20	11.99	1.01	0.88	0	0.1065	59.06	7.27	3.56
7-10	17.72	498.55	84.61	1.50	11.55	1.38	0.94	0	0.2025	29.59	2.61	1.00
7-11	17.66	498.45	84.51	1.42	11.73	1.28	1.07	0	0.2025	44.14	3.60	1.69
7-12	17.57	498.45	84.61	1.36	11.68	1.24	1.11	0	0.2025	58.37	4.64	2.33
7-13	19.96	498.55	85.20	1.02	11.65	1.32	0.81	0	0.1023	30.10	5.03	1.74
7-14	19.96	498.55	83.92	2.31	11.66	1.24	0.87	0	0.1023	45.36	7.13	2.81
7-15	19.96	498.55	84.65	1.56	11.75	1.13	0.92	0	0.1023	59.59	8.48	3.89
7-16	22.25	498.45	84.58	1.42	11.85	1.30	0.82	0	0.1065	29.62	4.69	1.65
7-17	22.34	498.65	84.70	1.35	11.83	1.25	0.85	0	0.1065	44.10	6.68	2.56
7-18	22.47	498.65	84.66	1.28	11.94	1.19	0.93	0	0.1065	59.83	8.62	3.78

9.3 Derivation using Matlab

The parameters were estimated using the following in Matlab 2011b:

```
%Main program
clear all
clc
global R

disp('Start calculation')

R = 8.314;              % gas constant (J/mol/K)
Tatmos = 298;           % atmospheric in K
Patmos = 1;             % atmospheric pressure in bar
MwMeOH = 32;            % Molecular weight methanol
MwH2O = 18;             % Molecular weight water
WF = 1;                 % Weighing factor
kk = [Data];            % Kinetic table

Parameter = zeros(126,11);

for j=1:42
    phi = kk((3*(j-1)+1):(3*j),11);
    RMeOHreal = kk((3*(j-1)+1):(3*j),12);
    RH2Oreal = kk((3*(j-1)+1):(3*j),13);

    for i = 1:3
        y = kk(3*(j-1)+i,4:9);
        tt = kk(3*(j-1)+i,3);
        press = kk(3*(j-1)+i,2);

        [phi_coeff] = fugacity(y)
        fug = y.*phi_coeff*(press*10^6);
        [Kp1 Kp2 Kp3]=chemkp(tt);

        r1 =  (model dependent equation)
        r2 =  (model dependent equation)
        r3 =  (model dependent equation)


        MeOHfun = @(x,xdata)(r1+r3)*xdata;
        H2Ofun = @(x,xdata)(r2+r3)*xdata;
        x0 = [estimated parameters];

        [m]=lsqcurvefit(MeOHfun,x0,phi,RMeOHreal);
        [w]=lsqcurvefit(H2Ofun,x0,phi,RH2Oreal);

    end
end

feest=zeros(126,2);
k=1;
l=1;

for k=1:126
    ep = Parameter(k,:);
    for l = 1:126
        y = kk(l,4:9);
        tt = kk(l,3);
        press = kk(l,2)*10;
        [phi_coeff]=fugacity(y)
```

```
        fug = y.*phi_coeff*(press);
        [Kp1 Kp2 Kp3]=chemkp(tt);
        phiv = kk(l,11);

        r1 =  (model dependent equation)
        r2 =  (model dependent equation)
        r3 =  (model dependent equation)

        RMeOHcalc = (r1+r3)*phiv;
        RH2Ocalc = (r2+r3)*phiv;
        feest(126*(k-1)+l,1) = RMeOHcalc;
        feest(126*(k-1)+l,2) = RH2Ocalc;
        l=l+1;
    end
    k=k+1;
end

statistiek = zeros(126,5);

for q = 1:126
    rmeohr = kk(:,12);
    rh2or = kk(:,13);
    rmeohc = feest(126*(q-1)+1:126*q,1);
    rh2oc = feest(126*(q-1)+1:126*q,2);

    SSR = sum((rmeohc-rmeohr).^2+WF*(rh2oc-rh2or).^2);
    varm = std(rmeohc-rmeohr);
    varw = std (rh2oc-rh2or);
    averrorm = max(abs((rmeohc-rmeohr)./rmeohr)*100);
    averrorw = max(abs((rh2oc-rh2or)./rh2or)*100);

    statistiek(q,1) = SSR;
    statistiek(q,2) = varm;
    statistiek(q,3) = varw;
    statistiek(q,4) = averrorm;
    statistiek(q,5) = averrorw;

    q=q+1;
end


function [phi_coeff]=fugacity(y)
global R

%           H2      CO      CO2     Me0H    H2O     CH4
Tc      = [ 33.2   132.9  304.1   512.6   647.3   190.4 ];
Pc      = [ 13.0   35.0   73.8    80.9    221.2   46.0  ];
omega   = [ -0.218 0.066  0.239   0.556   0.344   0.011 ];
pol     = 0;
Tr      = tt./Tc;

mi      = (0.48+1.574.*omega)-(0.176.*omega.^2);

aci     = ((R^2.*Tc.^2)./Pc)*0.42747;
alfai   = (1+(mi.*(1-sqrt(Tr)))-(pol.*(1-Tr).*(0.7-Tr))).^2;
ai      = aci.*alfai;
a       =(sum(y.*sqrt(ai)));

bi      = 0.08664.*(R.*Tc)./Pc;
b       = sum(y.*bi);
```

```
A       = (a*((press)))/(R^2*(tt)^2);
B       = (b*((press)))/(R*(tt));

m = (A-B-B^2);
n = -A*B;
p = [1 -1 m n];
Z = (roots(p));
ZV = max(Z(imag(Z) == 0));

phi_coeff = exp((bi./b).*(ZV-1)-log(ZV-B)+(A./B).*(bi./b-2*sqrt(ai./a))*log(1+B./ZV));

end

function [Kp1 Kp2 Kp3] = chemkp(tt)

Kp1 = 10.^(5139./(tt)-12.621);
Kp2 = 10.^(-2073./(tt)+2.029);
Kp3 = Kp1.*Kp2;

end
```